

1 Mountain permafrost in the Central Pyrenees: insights from
2 the Devaux ice cave

3 Miguel Bartolomé^{1*}, Gérard Cazenave², Marc Luetscher³, Christoph Spötl⁴,
4 Fernando Gázquez^{5,6}, Ánchel Belmonte⁷, Alexandra V. Turchyn⁸, Juan Ignacio
5 López-Moreno¹, Ana Moreno¹

6 1 Departamento de Procesos Geoambientales y Cambio Global, Instituto
7 Pirenaico de Ecología-CSIC, Zaragoza, Spain.

8 2 Société de Spéléologie et de Préhistoire des Pyrénées Occidentales
9 (SSPPO), 5 allée du Grand Tour, 64000 PAU, France

10 3 Swiss Institute for Speleology and Karst Studies (SISKA), La Chaux-de-
11 Fonds, Switzerland

12

13 4 Institute of Geology, University of Innsbruck, 6020 Innsbruck, Austria

14 5 Water Resources and Environmental Geology Research Group, Department
15 of Biology and Geology, University of Almería, Almería, Spain.

16

17 6 Andalusian Centre for the Monitoring and Assessment of Global Change
18 (CAESCG), University of Almería, Almería, Spain.

19

20 7 Sobrarbe-Pirineos UNESCO Global Geopark. Boltaña. Spain.

21 8 Godwin Laboratory for Palaeoclimate Research, Department of Earth Sciences,
22 University of Cambridge, Cambridge, UK

23

24 *Correspondence: Miguel Bartolomé (mbart@ipe.csic.es)

25

26 **Abstract (250 words)**

27 Ice caves are one of the least studied parts of the cryosphere, particularly those
28 located in inaccessible permafrost areas at high altitudes or high latitudes. We
29 characterize the climate dynamics and the geomorphological features of Devaux
30 cave, an outstanding ice cave in the Central Pyrenees on the French-Spanish
31 border. Two distinct cave sectors were identified based on air temperature and

32 geomorphological observations. The first one comprises well-ventilated galleries
33 with large temperature oscillations likely influenced by a cave river. The second
34 sector corresponds to more isolated chambers, where air and rock temperatures
35 stay below 0°C throughout the year. Seasonal layered ice and hoarfrost occupy
36 the first sector, while transparent, massive perennial ice is present in the isolated
37 chambers. Cryogenic calcite and gypsum are mainly present within the perennial
38 ice. During winter, the cave river freezes at the outlet, resulting in a damming and
39 back-flooding of the cave. We suggest that relict ice formations record past
40 damming events with subsequent formation of congelation ice. $\delta^{34}\text{S}$ values of
41 gypsum indicate that the sulfate originated from the oxidation of pyrite present in
42 the bedrock. Several features including ~~the~~ air and rock temperatures, the
43 absence of drips, the low-small loss of ice in the past seven decades, and the
44 location of ice bodies in the cave indicate that the cave permafrost is the result of
45 a combination of undercooling by ventilation and diffusive heat transfer from the
46 surrounding permafrost, reaching a thickness of ~200 m ~~below the surface~~.

47 **Keywords:** Ice cave, cave monitoring, cryogenic cave carbonates, cryogenic
48 gypsum, ~~Devaux cave~~ Pyrenees.

49 1. Introduction

50 Mountain areas are ~~one of the most susceptible among those~~ environments ~~to~~
51 most affected by current climate change (Hock et al., 2019). In the mid-latitudes,
52 high-altitude areas are subject to mountain permafrost, a very sensitive and
53 unstable phenomenon that responds quickly to environmental changes (Harris et
54 al., 2003; Biskaborn et al., 2019) due to the number of factors. ~~They influence the~~
55 ~~spatial distribution of mountain permafrost, including snow cover distribution and~~
56 ~~thickness, topography, water availability, surface temperature and rock~~
57 ~~temperature~~ Snow cover distribution and thickness, topography, water availability,
58 and surface and rock temperature influence the spatial distribution of mountain
59 permafrost (Gruber and Haeberli, 2009). ~~In light of these processes, Due to this~~
60 ~~number of processes~~ multidisciplinary studies including, among others,
61 measurements of rock temperature ~~measurements~~ in boreholes, ~~and the~~ bottom
62 temperatures of snow cover (BTS), ~~a variety of~~ geophysical techniques, and
63 ~~thematic detailed maps mapping~~ (geomorphology, thermal) are needed to gain a

Comentado [M1]: Reviewer #2.
155-57: (R) snow cover distribution and thickness, topography, water availability, surface and rock temperature all influence the spatial distribution of mountain permafrost

Comentado [M2]: Reviewer #2.
157-61: (R) In light of these processes, [...] are needed to gain a comprehensive understanding of mountain permafrost.

64 comprehensive understanding of mountain permafrost (e.g. Lewkowicz and
65 Ednie, 2004; Serrano et al., 2019; Biskaborn et al., 2019). On the other hand, ~~the~~
66 integrated study studies of paleo-permafrost (e.g. ~~Vaks et al., 2020~~), e.g. Vaks et
67 al., 2020 and modern permafrost, specifically mountain permafrost (e.g., Supper
68 et al., 2014; Scandroglio et al., 2021), sheds light on past, present and future
69 developments of permafrost areas, an issue of vital importance in the context of
70 global warming. Studies of past permafrost require sedimentary records, which
71 are locally preserved in caves located at high altitudes and/or high latitudes.

72 ~~Thus, temporal and spatial changes in past permafrost distribution have been~~
73 identified using speleothems (stalagmites, flowstones) in high-
74 latitude circumpolar and polar regions (e.g., Vaks et al., 2013, 2020; Moseley et
75 al., 2021; Li et al., 2021) as well as in mid-latitude regions (e.g., Lundberg and
76 McFarlane, 2007; Fankhauser et al., 2016; Lechleitner et al., 2020).

77 Ice caves are ~~defined as~~ cavities in rock hosting perennial ice that results from
78 the transformation of snow and/or the freezing of infiltrating water reaching the
79 cave (Perşoiu and Lauritzen, 2018). Cave ice can be dated and used as a
80 valuable paleoclimate archive in non-polar areas (e.g., Stoffel et al., 2009; Spötl
81 et al., 2013; Perşoiu et al., 2017; Kern et al., 2018; Sancho et al., 2018a; Leunda
82 et al., 2019; Munroe, 2021; Racine et al., 2022).

83 ~~Furthermore, temporal and spatial changes in past permafrost distribution have been identified using~~
84 ~~speleothems (stalagmites, flowstones) in circumpolar and polar regions (e.g., as~~
85 ~~well as in mid-latitude regions (e.g., Lundberg and McFarlane, 2007; Fankhauser~~
86 ~~et al., 2016; Lechleitner et al., 2020).~~ Recently, coarse cryogenic cave carbonates
87 (CCC_{coarse}), that form during slow freezing of water inside caves, have been used
88 as indicator of permafrost degradation, permafrost thickness, and subsurface ice
89 formation (Žák et al., 2004, 2012; Richter et al., 2010a; Luetscher et al., 2013;
90 Orvošová et al., 2014; Spötl and Cheng, 2014; Bartolomé et al., 2015;
91 Dublyansky et al., 2018; Koltai et al., 2020; Munroe et al., 2021; Spötl et al.,
92 2021).

93 Many ice caves are located in areas where the mean annual air temperature
94 (MAAT) outside the cave is above 0°C (Perşoiu and Lauritzen, 2018) and,
95 therefore, are highly susceptible to future climate warming (Kern and Perşoiu,
96 2013). These ice caves are local thermal anomalies which are controlled by the

Comentado [M3]: New reference added:

Li, T.-Y., Baker, J. L., Wang, T., Zhang, J., Wu, Y., Li, H.-C., Blyakharchuk, T., Yu, T.-L., Shen, C.-C., Cheng, H., Kong, X.-G., Xie, W.-L., and Edwards, R. L.: Early Holocene permafrost retreat in West Siberia amplified by reorganization of westerly wind systems, *Commun. Earth Environ.*, 2, 1–11, <https://doi.org/10.1038/s43247-021-00238-z>, 2021.

Comentado [M4]: Reviewer#1: lines 73-78: This sentence somehow doesn't fit to the other parts of this paragraph. Please consider omitting it or moving it to another place where it fits better.

Con formato: Inglés (Estados Unidos)

Comentado [M5]: added:

Racine, T. M. F., Reimer, P. J., and Spötl, C.: Multi-centennial mass balance of perennial ice deposits in Alpine caves mirrors the evolution of glaciers during the Late Holocene, *Sci. Rep.*, 12, 11374, <https://doi.org/10.1038/s41598-022-15516-9>, 2022.

Con formato: Inglés (Estados Unidos)

Código de campo cambiado

Comentado [M6]: Moved from here to lines 70-75

Comentado [M7]: New reference added:

Spötl, C., Koltai, G., Jarosch, A. H., and Cheng, H.: Increased autumn and winter precipitation during the Last Glacial Maximum in the European Alps, *Nat. Commun.*, 12, 1839, <https://doi.org/10.1038/s41467-021-22090-7>, 2021.

97 cave geometry and the associated ventilation pattern. Their ice deposits
98 represent sporadic permafrost occurrences and do not inform about the wider
99 thermal environment. In contrast, at high altitudes and high latitudes subsurface
100 ice deposits are still preserved by the presence of permafrost under the current
101 climate-conditionchange. There, mountain permafrost is limited to areas where
102 a periglacial belt is present, with MAAT $\leq 0^\circ$ C. For example, in the European
103 Alps, discontinuous mountain permafrost is observed between-above 2600 and
104 to 3000 m a.s.l. (Boeckli et al., 2012), while in southern Europe permafrost is
105 generally absent (i.e. not observed even on the highest massif of the Iberian
106 Peninsula, Gómez-Ortiz et al., 2019). In the Central Pyrenees few studies
107 suggest the possible presence of permafrost above 2750 m a.s.l. (Serrano et al.,
108 2019, 2020; Rico et al., 2021), and the presence of a few ice caves has only
109 recently been documented (e.g. Sancho et al., 2018a; Serrano et al., 2018)
110 informing about the occurrence of sporadic permafrost.-

111 The aim of this study is to characterize the permafrost conditions in Devaux cave,
112 a high-altitude ice cave in the Central Pyrenees. We monitored air, water and
113 rock temperatures and used cryogenic cave deposits to i) document the
114 distribution of permafrost within this cave, and ii) to study the processes that
115 resulted in perennial cave ice bodies and associated cryogenic mineral
116 occurrences.

117

118 2. Study site

119 Devaux cave opens at ~2838 m a.s.l. in the NE cliff of Gavarnie cirque (France)
120 of the Monte Perdido massif (MPm) in the Central Pyrenees (Fig. 1a). The cave
121 is located between the Parc National des Pyrénées (France) and the Parque
122 Nacional de Ordesa y Monte Perdido (Spain). Named after Joseph Devaux who
123 discovered and explored it in 1928, the cave was later investigated with respect
124 to its hydrogeology and microclimatology and preliminary descriptions of its
125 deposits were reported (e.g., Devaux, 1929; 1933; Rösch and Rösch, 1935;
126 Rösch, 1949; dDu Cailar and Dubois, 1953; Requirand, 2014).

127

Comentado [M8]: Reviewer #2

A)I90-91:

In contrast, at high altitudes and high latitudes ice deposits are still preserved under the current climate change may be in relation to the permafrost presence.

Done

Comentado [M9]: Reviewer #2

I98-99: (T) the presence of a few ice caves has only recently been documented

Done

Comentado [M10]: Reviewer #2

B) I98-99:

), informing about sporadic permafrost

Done

128 The area is dominated by limestones and dolostones ranging from the Upper
129 Cretaceous to the Eocene-Paleocene. MPM is the highest limestone karst area
130 in Europe reaching up to 3355 m a.s.l. (Monte Perdido peak) (Fig. 1b). The
131 nearest peaks to Devaux cave are Marboré (3248 m a.s.l.) and the three Cascada
132 peaks (3164 m, 3111 m, and 3098 m a.s.l.). The limestone thickness above the
133 cave varies between ~200 and 250 m (Fig. 2a). In Devaux, the galleries follow
134 the axis of a NW-SE striking syncline (Fig. 1b). A river runs along the cave (Fig.
135 2a, b). The cave has two known entrances: the lower one corresponds to the
136 main outlet of the cave river (Brulle spring, North 1, ~2821 m a.s.l.), while the
137 upper entrance is known as the “Porche” (South, ~2836 m a.s.l.) (Figs. 1c and
138 2b). Between these two entrances, a small gallery (Spring North 2) opens +1.2 m
139 above Brulle spring (Fig. 1c). Brulle is one of the main springs in the Gavarnie
140 cirque. This spring drains a catchment of ~2.6 km² (polje) located on the southern
141 face of MPM between ~2850 and 3355 m a.s.l. (Figs. 1b and, 1d). Major water
142 flow is observed during late spring and early summer when snowmelt ~~recharges~~
143 occurs in a catchment characterised by shafts, sinkholes and small closed
144 depressions (Fig. 1d). The water of Brulle spring feeds, together with some other
145 springs located a few hundred meters below, the Gavarnie waterfall (Fig. 1b). A
146 tracer experiment (du Cailar et al., 1953) indicated that part of the water of the
147 Gavarnie waterfall, and thus likely also from Brulle spring, comes from a ponor in
148 the Lago helado (lake, Fig. 1e); located ~2.3 km to the east of Devaux cave (Figs.
149 1b and 2a). The Gavarnie waterfall (Fig. 1b) turned green within ~21 hours after
150 injection of the tracer but the water at Brulle spring was not directly checked (du
151 Cailar et al., 1953). During the colder months, the spring ~~water~~ as well as the
152 Gavarnie waterfall freeze.

153 The geomorphology of the area is dominated by karst, glacial and periglacial
154 landforms. The area was strongly glaciated during the last glacial period on both
155 sides of the massif (e.g., Reille and Andrieu, 1995; Sancho et al., 2018b;
156 Bartolomé et al., 2021). Today, only two glacier relicts covered by scree deposits
157 are present in the Gavarnie cirque (Fig. 1b): 1) the Cascada dead-ice which is
158 located several hundred meters below Devaux cave, and 2) a dead-ice
159 accumulation in the NE wall of the cirque. Till present close to Brulle spring, on
160 the access to Devaux and in the Cascada glacier, point to a much larger glacier

Con formato: Inglés (Estados Unidos)

161 extent in the past, maybe corresponding to the Little Ice Age or even the
162 Neoglacial advance recognized in the nearby Tucarroya (Fig. 1b) and Troumouse
163 cirques (Gellatly et al., 1992; González Trueba et al., 2008; García-Ruiz et al.,
164 2014, 2020).

Con formato: Inglés (Estados Unidos)

165 The study area lies at the transition between Atlantic and Mediterranean climate,
166 with generally cold and dry winters and warm and dry summers. In MPm, the
167 annual ~~zero~~ 0°C isotherm is located at ~ 2900 m a.s.l. (López-Moreno et al., 2016;
168 Serrano et al., 2019). The wet seasons are fall and spring. The annual
169 precipitation at the Góriz meteorological station (2150 m a.s.l. and 3 km SE of the
170 cave) averages 1650 mm. ~~However, mass balance calculations of the nearby~~
171 ~~Monte Perdido glacier, where more than 3 m of snow (density ~~e~~ 450 kg/m³)~~
172 ~~accumulates between November to April, indicates a minimum amount of 1500~~
173 ~~mm w.e (water equivalent), therefore the total annual precipitation in~~ elevate high
174 ~~areas parts of the massif exceedsss 2500 mm~~ However, mass balance
175 ~~calculations of the nearby Monte Perdido glacier suggest that annual precipitation~~
176 ~~next to the cave may exceed 2500 mm, as the snow depth measured in early~~
177 ~~May exceeds on average 3 m (López-Moreno et al., 2019).~~ In the MPm,
178 discontinuous permafrost is present between ~2750 and ~2900 m a.s.l. and
179 becomes more frequent above ~2900 m a.s.l. on the northern side (Serrano et
180 al., 2019). Periglacial activity is characterized by rock glaciers, solifluction lobes
181 and patterned ground (Feuillet, 2011).

Con formato: Inglés (Estados Unidos)

182

183 3. Material and methods

184 3.1 Cave survey and mapping

185 A survey of Devaux cave was conducted using a compass and clinometer as well
186 as a laser distometer (Disto-X, Heeb, 2014). In addition to cave ice, chemical and
187 clastic deposits were mapped inside the cave. ~~These features were overlain onto~~
188 ~~the cave survey to produce a geomorphological cave map~~ (Fig. 2b). The labelling
189 of the cave chambers (A to K) follows the nomenclature introduced by Devaux
190 (1929) and Rösch and Rösch (1935).

191 A map of potential solar radiation (RAD) of the MPm was obtained using an
192 algorithm which considers the effects of the surrounding topography on
193 shadowing considering the position of the sun. RAD was calculated for every
194 month ~~of the year~~ and was then averaged to obtain an annual mean. Details of
195 this computation can be found in [Pons and Ninyerola \(2008\)](#).

196 3.2 Cave monitoring

197 The cave consists of large rooms (e.g., room F, ~~or and~~ those located beyond
198 SCAL chatière) connected by small galleries (Fig. 2b), locally with narrow
199 passages (e.g., galleries close to SPD room or SCAL chatière, Fig. 2b). 15
200 stations were installed in the outmost ~350 m of the cave to monitor air (11
201 sensors), water (2 sensors) and rock temperature (2 sensors) (Fig. 2b). Cave air
202 temperature variations were recorded using different devices (Hobo Pro v2 U23-
203 001 (accuracy $\pm 0.25^\circ\text{C}$, resolution 0.02°C), Tinytag Talk 2 (accuracy $\pm 0.5^\circ\text{C}$,
204 resolution, 0.04°C) and ELUSB2 (accuracy $\pm 0.21^\circ\text{C}$, resolution 0.5°C). The cave
205 river temperature was recorded at two points. ~~T;~~ the first site (W7) was located
206 close to the Brulle spring (Fig. 2b; Hobo TiDBit V2, accuracy $\pm 0.21^\circ\text{C}$, resolution
207 0.02°C) and, the second site (W6) was located in room F (Fig. 2b; Hobo UA-001-
208 08; accuracy $\pm 0.53^\circ\text{C}$, resolution 0.4°C). Both sensors were installed at a water
209 depth of 20 cm. Finally, the rock temperature was recorded at two sites (R1 and
210 R2 in room D and K, respectively) using a Hobo U23-003 device (accuracy
211 $\pm 0.25^\circ\text{C}$, resolution 0.02°C). Each sensor has two external temperature probes
212 (channels 1 and 2, Ch1-Ch2). These temperature probes were installed in two
213 horizontal drill holes of 60 cm depth, ~1.5 to 2 m from each other.

214 We monitored sporadically the cave during different ~~time~~ intervals between 2011
215 and 2015, while a continuous monitoring was carried out between July 2017 and
216 July 2021. ~~We calculated the m~~Maximum, minimum and mean temperatures as
217 well as the number of frost/warm days were obtained for each sensor and site
218 (Fig. 2b). Changes in the ice morphology were evaluated using wall marks
219 measured at four points since 2013 in room G and using one point during 2020-
220 2021 in room SPD (Fig. 2b) using a digital sliding caliper.

221 The outside temperature was measured at ~~two points in the MPm, at~~ the “Porche”
222 entrance (~2836 m a.s.l.) and on the southern face of MPM at ~2690 m a.s.l. For

Comentado [M11]: Reviewer #2
C) l183:

223 comparison, these temperature records were corrected assuming an adiabatic
224 lapse rate of ~~0.55°C 100+5.5 °C km⁻¹ m~~ (López-Moreno et al., 2016; Navarro-
225 Serrano et al., 2018) to an elevation of ~2850 m a.s.l., corresponding
226 approximately to the lower limit of the hydrological catchment area of Devaux. In
227 both cases, the temperature was measured using Tinytag Talk 2 sensors
228 equipped with a radiation shield. These data were compared to the temperature
229 record from the Pic du Midi de Bigorre meteorological station (PMBS; 2011-
230 2020) (2860 m a.s.l., ~28 km N of Devaux) obtained from Météo-France.
231 Moreover, the homogenised MAAT dataset available since 1882 from PMBS
232 (Bücher and Dessens, 1991; Dessens and Bücher, 1995) ~~was-were~~ used to
233 identify-identify long-term climatic-temperature trends.

234 3.3 Mineralogy, water and mineral sampling X-ray diffraction, ion chromatography 235 and sulfur isotopes

236 X-ray diffraction (XRD) analyses were performed on sulfate and carbonate
237 crystals from rooms G, D and K, as well as on sulphide and oxidized crystals
238 thereof from the host rock (Fig. S1). The analyses were performed at the
239 Geosciences Institute in Barcelona (GEO3-BCN-CSIC) using a Bruker-AXS
240 D5005 powder diffractometer configured in ~~θ/2θ-model~~ (e.g. Rodríguez-Salgado
241 et al., 2021) ~~theta-2 theta geometry~~.

242 Samples of cave drips water, ice and river water were analysed for major ions by
243 ion chromatography (IC) at the laboratories of the Pyrenean Institute of Ecology
244 (Zaragoza). Carbonate alkalinity was determined by titration within 24 hours after
245 sampling.

246 Sixteen samples, including sulfate crystals, dissolved sulfate and pyrite crystals
247 were selected for sulfur isotope analyses at the Godwin Laboratory for
248 Paleoclimate Research of the University of Cambridge (UK), following the
249 methodology of ~~Giesemann et al., (1994)~~. For gypsum samples, ~5 mg of
250 powdered gypsum were dissolved in deionized water at 45°C overnight. Then, a
251 BaCl₂ solution (50 g/L) was added to induce BaSO₄ precipitation. In the case of
252 water samples, BaCl₂ was added directly to the sample. Subsequently, 6M HCl
253 was added to remove ~~any co-precipitated~~ carbonate ~~minerals~~ and the BaSO₄
254 precipitate was rinsed several times with deionized water. Finally, BaSO₄ was

Comentado [M12]: Reviewer #1
line 210: I suggest expressing the lapse rate as 5.5°C km⁻¹ because the current expression is confusing. It suggests 0.55°C change by 0.01 m.

Comentado [M13]: Reviewer #1
line 214: Please capitalize "Midi"

Comentado [M14]: Reviewer #1:
The title of sub-section 3.3 needs revision. The current title is misleading. The section is not about sampling but about the methodology of the applied mineralogical and geochemical analyses.

Comentado [M15]: Reviewer #1:
An additional related comment is that it is stated in section 4.4.2 that "XRD analyses yielded ...gypsum, calcite, ... pyrite and goethite," however no evidence is presented. I suggest adding some annotated diffractograms (at least in a supplementary document) in the revised version.

Comentado [M16]: Reviewer #1
line 244: Maybe "Bragg-Brentano geometry" or "θ/2θ-mode" would be the appropriate expression.

Comentado [M17]: Reference added.
Rodríguez-Salgado, P., Oms, O., Ibáñez-Insa, J., Anadón, P., Gómez de Soler, B., Campeny, G., and Agustí, J.: Mineralogical proxies of a Pliocene maar lake recording changes in precipitation at the Camp dels Ninots (Pliocene, NE Iberia), *Sedimentary Geology*, 418, 105910, <https://doi.org/10.1016/j.sedgeo.2021.105910>, 2021.

Con formato: Color de fuente: Énfasis 1

Código de campo cambiado

Comentado [M18]: Reviewer #1:
It is also quite strange that there is not any reference for the applied methods. Please consider citing the proper references in the revised manuscript.

Comentado [M19]: Reference added:
Giesemann, A., Jaeger, H.-J., Norman, A. L., Krouse, H. R., and Brand, W. A.: Online Sulfur-Isotope Determination Using an Elemental Analyzer Coupled to a Mass Spectrometer, *Anal. Chem.*, 66, 2816-2819, <https://doi.org/10.1021/ac00090a005>, 1994.

255 dried at 45°C overnight. Sulfates dissolved in water were precipitated using the
256 same method.

257 Isotope measurements were carried out using a Flash Elemental Analyzer (Flash-
258 EA) at 1030 °C. The samples were folded in tin capsules. After sample
259 combustion, the generated SO₂ was measured by continuous-flow gas source
260 isotope ratio mass spectrometry (Thermo Scientific, Delta V Plus). Samples were
261 run in duplicate and calibration was accomplished using NBS-127. The
262 reproducibility (1σ) of δ³⁴S was better than 0.2‰, similar to the long-term
263 reproducibility of the standard over the run (0.2‰). δ³⁴S isotope values are
264 reported relative to VCDT (Vienna-Canyon Diablo Troilite).

265

266 **4. Results**

267 **4.1 Devaux cave description**

268 Devaux cave is ~2500 m long and comprises three distinct levels (Fig. 2b). The
269 lower and the middle levels correspond to the Brulle spring (0 m), and the
270 “Porche” entrance (~+14.5 m), respectively. The third one comprises chambers
271 and galleries +21 m to +29 m above the Brulle spring (Fig. 2b). In the inner part
272 of the cave, some unexplored vertical chimneys may connect to sinkholes in the
273 catchment above the cave (Fig. 2a). The main ice deposits are located in rooms
274 D, G, SPD and K (Fig. 2b). Except for SPD, these chambers located above the
275 Porche entrance (between ~+1 and +7 m) can be accessed via ascending
276 passages.

277 During the cold season, the cave river starts freezing at the spring and the ice
278 then expands backward into room F (Fig. 2b). The ice totally or partially clogs the
279 main gallery and dams the water inside the cave forming a small lake (cf. also
280 [Rösch and Rösch, 1935](#)). This process is important for the seasonal ice extent
281 as the flooding of the cave depends on whether the springs (North 1 and North
282 2) are frozen or not (e.g., [Rösch and Rösch, 1935](#)). Webcam observations
283 (Gavarnie, Oxygène hut) suggest a possible freezing of the Brulle spring from
284 late November to mid-May simultaneous with the freezing of the Gavarnie
285 waterfall. Moreover, historical photos (e.g., [Devaux, 1929](#); [Rösch and Rösch,](#)
286 [1935](#)) and our own observations show that snow during winter and spring can

287 reach the Brulle entrance - a situation that also favours the blocking of the
288 springs. As a result of such flooding events, slackwater deposits ~~are~~
289 ~~present~~formed in the cave entrance zone, but locally also further into the cave
290 (e.g., in rooms I, J, K and SCAL chatière, along the main gallery; Fig. 2b), while
291 silty sediments are found at elevated positions with respect to the river level (e.g.,
292 in rooms D and G). Sandy sediments dominate in the large rooms located beyond
293 the SCAL chatière. Two such successions (~1 m thick) comprising hundreds of
294 rhythmic fine sand- and silt layers are present in elevated areas with respect to
295 the current river, witnessing major events of back-flooding.

296 Observations made during summer show a dominant air-flow direction from the
297 inner to the outer parts of the cave, exiting through the Brulle and Porche
298 entrances. Conversely, the opposite is expected for the cold season (chimney
299 effect). When the Brulle spring is partially clogged by ~~the~~ ice during early summer
300 forcing the stream to flow below the ice, air flows from room F to C (Fig. 2b) (e.g.,
301 summer 2021). The air flow is imperceptible in rooms D, G, and close to K located
302 away from the main cave passages.

303 4.2 Climate setting of Devaux cave

304 The MAAT at the elevation of Devaux cave is ~0 °C (-0.04 °C; 2017-2021). On
305 the other hand, a positive MAAT (1.8 °C) is recorded on the southern side of the
306 MPm at a similar altitude (Fig. 3a). Maximum and minimum air temperatures
307 outside the cave vary between 24.5 °C and -17.2 °C (hourly values, 2017-2021).
308 The PMBS MAAT record (Fig. 3b) shows ~~an increase warming trend of~~ →around
309 +1.5 °C since the beginning of the measurements in 1882. Before 1985,
310 temperatures below 0°C dominated the annual cycle, while positive MAATs
311 became more frequent in recent years. Minimum temperatures also show ~~a~~
312 ~~temperature—~~increasing trend of ~+2.5 °C, while the maximal annual
313 temperatures do not show a clear trend. The north-facing Gavarnie cirque is
314 associated with a clear RAD anomaly (Fig. 4). Values lower than 215 kWh/m² are
315 observed at ~2000 m and between ~2800 and 2900 m a.s.l., corresponding to
316 the cirque bottom, the area located behind La Torre peak and the surroundings
317 of Devaux cave. At the cave site-entrance the RAD value is only 390 kWh/m², in

Comentado [M20]: Reviewer #2

line 290: Please explain it a bit more what is “an increase of ~+1.5 °C”. A trend value? or the difference between the mean of a certain period at the beginning and at the end of the record? or what?

Comentado [M21]: Reviewer #2

line 299: Please check the dimension.

318 stark contrast to the summit areas and surroundings where the RAD often
319 exceeds 1500 kWh/m² (Fig. 4).

320 While the mean daily air temperature (MDAT) at the cave entrance (purple line in
321 Fig. 5) and the temperature series from PMBS (pink line in Fig. 5) agree in their
322 absolute values, the variability of MDAT at the Devaux entrance is lower than at
323 the PMBS. This pattern could be related to local topographic conditions leading,
324 for instance, to less RAD, or to the position of the sensor in the cliff (less night
325 emissivity). Given this radiation contrast, warmer temperatures prevail on the
326 southern side of the MPm (Fig. 4), favouring early snowmelt in spring and early
327 summer, while at the same time the temperature stays below 0 °C in the cave's
328 surroundings.

329 4.3 Devaux cave temperature variations

330 The cave can be separated into distinct areas depending on their thermal regime:
331 ventilated galleries (rooms A, B, C, F and the main gallery from SPD to SCAL
332 chatière) ~~to K~~) and ~~these poorly ventilated parts~~ off the main air flow path (rooms
333 D, G, K - Figs. 2b, 5).

334 4.3.1 Well-ventilated cave parts

335 Air (T_{2air}, T_{5air}, T_{10air}, T_{11air}) and water (W_{6water}, W_{7water}) temperature data show
336 large seasonal oscillations. ~~at T_{2air}, T_{5air}, T_{10air}, T_{11air}, T_{12air}, W_{6water}, W_{7water} and~~
337 ~~R_{2rock} sensors.~~ All sensors except T_{11air}, ~~T_{12air}, and R_{2rock}~~ show a few days with
338 of positive temperatures during summer. Sensor T_{2air} (2011-2012, Fig.5a), which
339 is also the closest to the Porche entrance, shows the highest correlation (r) with
340 the external temperature (0.73, p<0.001). Sensor T_{5air} (2017-2021, Fig. 5d) in
341 room B also shows a high correlation and significant correlation (0.82, p<0.0005)
342 with the outside temperature. During the major cave refrigeration/cooling that
343 takes place between the end of October ~~to~~ and May and the correlation is
344 significatent and ranges between 0.68 to 0.84. During ~~the~~ summers and part of
345 the falls, the correlations decreases notably (-0.23 to 0.76). ~~Sensor T_{11air} (2018-~~
346 ~~2021, Fig. 5d) is located in SPD room. Despite being a well-ventilated gallery, the~~
347 ~~sensor is relatively protected from the air flow by the room morphology and shows~~
348 ~~lower correlations (0.69, p<0.001)is partly protected from the air flow and shows~~
349 ~~lower a correlation (0.69, p<0.001) despite being located in a well-ventilated~~

Comentado [M22]: Reviewer #2

I315: I think this could be reformulated, as the authors list water, and rock T sensors together with the air T sensors.

Con formato: Color de fuente: Automático

Con formato: Color de fuente: Automático

350 gallery (SPD room). Also during the ~~refrigeration~~winter months, the correlations
351 are lower (0.49-0.62, $p < 0.001$) than in T5_{air}. ~~Sensor T5_{air} (2017-2021, Fig. 5d)~~
352 ~~in room B also shows a high correlation with the outside temperature from~~
353 ~~November to May (0.82, $p < 0.001$ (2017-2018); 0.66, $p < 0.001$ (2018-2019); 0.66,~~
354 ~~$p < 0.001$ (2019-2020); 0.86, $p < 0.001$ (2020-2021)), while during summer and fall~~
355 ~~correlations with external temperatures are slightly weaker (0.52, $p < 0.001$ (2017-~~
356 ~~2018); 0.37, $p < 0.001$ (2019-2020); 0.66 $p < 0.001$ (2020-2021)). Sensor T11_{air}~~
357 ~~(2017-2021, Fig. 5d) is located in SPD room. Despite being a well-ventilated~~
358 ~~gallery, the sensor is relatively protected from the air flow by the room morphology~~
359 ~~and shows lower correlations (0.45, $p < 0.001$ (2018-2019); 0.34, $p < 0.001$ (2019-~~
360 ~~2020); 0.79 $p < 0.001$ (2020-2021)) compared to T5_{air}. Sensor T10 (2014-2015,~~
361 ~~Fig. 5c) does not show any significant correlation with the external temperature.~~
362 ~~Sensors T12_{air} and R2_{rock} are located in room K, and similar to T11_{air}, the chamber~~
363 ~~morphology shields them from the air flow. Rock temperature sensor R2_{rock}~~
364 ~~shows a slightly variable temperature ranging between -0.10°C and 0.28°C~~
365 ~~(mean of -0.24 and -0.23°C for channel 1 and 2, respectively). Sensor T12_{air}~~
366 ~~shows a low correlation with the external temperature ($r^2 = 0.35$, $p < 0.001$ (2019-~~
367 ~~2021)), and the same is observed for T_{ext} - R2_{rock} ($r^2 = 0.35$, $p < 0.001$ (2019-~~
368 ~~2021)). Meanwhile the correlation between T12_{air} and R2_{rock} is high but not significant~~
369 ~~($r^2 = 0.93$, $p > 0.005$ (2019-2021)).~~

370 ~~The water s~~Sensors W6_{water} and W7_{water} (Figs. 5b, c) recorded water temperature
371 variations during the years 2012-2013 and 2014-2015, respectively. Both sensors
372 record a continuous temperature decline from the end of November to mid-
373 January until the water freezes. At W7_{water}, the temperature ranges between -0.3
374 and -5.8 °C between the end of fall and the beginning of winter, while between
375 January and the beginning of June, the temperature stays close to 0°C between
376 January and the beginning of June. At W6_{water}, the temperature reached a
377 minimum of -1.7 °C and shows smaller variations than at W7_{water}. No significant
378 correlation was found between the external air temperature and the river water
379 temperature. Only W6_{water} shows a weak small correlation with the external
380 temperature when ice is absent (0.39 $p < 0.001$ and 0.40 $p < 0.001$).

381 For each monitored interval, the mean annual cave temperature at the T2_{air}, T5_{air}
382 and T11_{air} sensors is lower than the outside mean temperature for the same

Comentado [M23]: line 346: I suggest replacing "small" with "weak".

383 ~~period (by 0.4°, 2.0°, 3.3° C lower, respectively). The W6_{water}, W7_{water} and T10_{air}~~
384 ~~sensors show mean temperatures higher than the external mean temperatures~~
385 ~~(by 1.6°, 2.6°, 2.5° C higher, respectively). The periods 2011-2012 and 2017-2018~~
386 ~~(at T2_{air} and T5_{air}, respectively) represent the coldest cave years of the monitoring~~
387 ~~period.~~

388

389 4.3.2 Poorly ventilated cave parts

390 ~~Air temperature s~~Sensors located in rooms D (T3_{air}, T4_{air}, T8_{air}, R1_{rock}), ~~and G~~
391 ~~(T9_{air}), K (T12_{air}), and rock temperature (R1_{rock}, R2_{rock}) show air temperatures~~
392 ~~below 0 °C during the monitoring period with small oscillations and a weak and/or~~
393 ~~insignificant correlation with the external air temperature. All sensors show~~
394 ~~temperatures below 0 °C during the monitoring period with small oscillations.~~
395 Sensor R1_{rock} (Fig. 5) recorded rock temperatures consistently below 0°C during
396 the entire monitoring period. This sensor shows constant rock temperatures (-
397 1.24 °C and -1.27 °C for channels 1 and 2, respectively), similar within error to
398 the cave air temperature (T3_{air}, T9_{air}; 2019-2021). All sensors except for T3_{air}
399 (2011-2012, Fig. 5a) show mean air and rock temperatures lower than the mean
400 external temperature during the same period (by 0.59 °C to 2.47°C lower). The
401 muted temperature variations in these chambers reflect reduced heat exchange
402 compared to the well-ventilated parts of the cave. Sensors T12_{air} and R2_{rock} are
403 located in room K, and similar to T11_{air}, the chamber morphology shields them
404 from the air flow. Rock temperature sensor R2_{rock} shows a slightly more variable
405 temperature ranging between -0.19°C and -0.28°C (mean of -0.24 and -0.23°C
406 for channel 1 and 2, respectively). Sensor T12_{air} shows a low correlation with the
407 external temperature ($r^2=0.35$, $p<0.001$ (2018-2021)), and the same is observed
408 for T_{ext} - R2_{rock} ($r^2=0.35$, $p<0.001$ (2019-2021)). Meanwhile the correlation
409 between T12_{air} and R2_{rock} is high but not significant ($r^2=0.93$, $p>0.005$ (2019-
410 2021)).

411

412

413 4.4 Cave deposits

Comentado [M24]: Reviewer #2
1357: I think R1 could be dropped from the list in parentheses,
as it is not an air temperature sensor.

414 **4.4.1 Ice**

415 Congelation ice formed by freezing of water within the cave is the most abundant
416 type of ice, and four main ice deposits are located in chambers D, G, SPD, and
417 K (Fig. 2b). The most relevant feature of these ice bodies is their [high](#)
418 transparency and massive aspect, i.e. the lack of layering (Figs. 6a, b).
419 Transparent ice is present on the ceiling, blocking chimneys, galleries and
420 fractures. The local loss of transparency is related to the presence of cryogenic
421 cave minerals and/or air inclusions (Figs. 6a, b, c, d).

422 A highly transparent ice deposit covers the southwest wall of room D and blocks
423 the access to a gallery (Fig. 6a). The height of this deposit reaches ~6 m, and its
424 base is located ~20 m above the Brulle spring. The thickness of this ice deposit
425 ranges from 4.5 to 14.5 m (horizontal laser measurements across the ice in the
426 gallery blocked by ice) and the estimated volume ranges from ~350 to ~710 m³.
427 Three unconformities marked by cryogenic minerals were identified in this ice
428 body.

429 In room G, an ice body (~25.8 to 29.6 m above the Brulle spring) is present on
430 the ceiling (Fig. 6b) and the estimated ice volume is ~180 m³. A comparison with
431 a historical photograph [shortly](#) before 1953 ([Casteret, 1953](#)) suggests that the ice
432 body has not changed significantly during the last ~69 years (Figs. 7a, b). Ice-
433 rock distances measured at four points, however, reveal small changes at three
434 of them. The first has retreated 9.8 mm since 2014 (mean 0.9 mm a⁻¹, n=2), the
435 second has retreated 19.2 mm since 2014 (mean 0.6 mm a⁻¹, n=5), and the third
436 one has retreated 15.8 mm since 2013 (mean 2.2 mm a⁻¹, n=7). At ~80 m from
437 the entrance, a small descending room (SPD) (Figs. 2b, 6c) hosts a small volume
438 of ice. Measurements between 2020 and 2021 indicate a retreat of 20 mm a⁻¹
439 (n=1). A last major ice deposit is present ~280 m from the entrance (room K),
440 where transparent and massive ice (~15.5 m above the Brulle spring) ~~is currently~~
441 ~~fills a filling a~~ cupula or chimney (Figs. 2b, 6d). Additional ice bodies are present
442 behind the SCAL chatière in the upper gallery (Fig. 2b), but they have not been
443 studied.

444 In contrast to these massive ice deposits, layered ice of seasonal origin is present
445 in small chambers adjacent to the river (E and F rooms) (Fig. 6e). This ice forms

Comentado [M25]: Reviewer #2
I396: (T) transparent and massive ice (~15.5 m above the Brulle spring) currently fills a cupula or chimney

446 sheets of ~~around~~about 10-15 cm in thickness which are present in room F and
447 nearby areas (Fig. 6f). This ice is related to the damming and freezing of water
448 inside the cave when the Brulle spring freezes. Our visits from 2017 to 2021
449 revealed that most of the damming and subsequent ice formation in room F took
450 place during winter and spring 2017-2018 corresponding with the coldest months
451 (both inside the cave and outside) of the monitoring period (Fig. 5d). These ice
452 slabs are characterized by flat surfaces on both sides and obviously record
453 incomplete freezing of the dammed water. The ice sheets largely disappeared
454 during summer and fall, and only strongly degraded ice remained in elevated
455 areas of room F.

456 On the other hand, ~~the~~ ice sheets associated with earlier episodes of river
457 damming and freezing have disappeared, and only linear colour changes
458 remained as witnesses of such events on the walls of the room E (Fig. 8d). A
459 historical photograph exemplifies these ice levels in the access between rooms
460 F and E (Fig. 8a). In August 1984 the ice was close to the ceiling and nearly 1 m
461 thick (Fig. 8a; Marc Galy, pers. comm.). This contrasts with the low ice level in
462 recent years (Fig. 8b). In total, three ice-level marks were identified in relation to
463 back-flooding and subsequent freezing of ponded water (Figs. 8c, d). They
464 appear at a lower elevation than the Porche entrance (c.+9.5, +9.2, +8.8, m with
465 respect to the Brulle spring).

466 Another important feature is the presence of hoarfrost, which ~~is~~was observed in
467 rooms A, B, C, E, F and along the gallery between SPD and ~~K-J~~ (Figs. 2b, 7g, ~~7h~~).
468 The crystal size varies from few mm to 4 cm and appears to be upholstering some
469 galleries and cupolas, forming aggregates that hang from the ceiling (Fig. 6h).
470 Finally, seasonal ice formations (e.g., icicles and ice stalagmites), as well as drips
471 are restricted to the outmost ~15 m, in the vicinity of both entrances, and in the
472 innermost part of the cave (~ 500 m from the entrance). Seasonal ice formations
473 are absent in cave sectors where transparent ice bodies and hoarfrost are
474 present. Firn deposits derived from snow are restricted to the Porche entrance.

475

476 **4.4.2 Mineral deposits**

477 They comprise mainly cryogenic cave minerals. XRD analyses of samples from
478 rooms D, G and K yielded gypsum and calcite, while the sulfide crystals and their
479 oxidation products present in the host rock were identified as pyrite and goethite,
480 respectively. The presence of cryogenic gypsum in Devaux was already reported
481 by du Cailar and Dubois (1953). In room D, gypsum was observed within the ice
482 and on boulders (Figs. 9a, b, c). A total of three gypsum levels (lower, middle and
483 upper, located at ~21.4, ~22.6 and ~23.9 m, respectively, with respect to the
484 Brulle spring) were identified in the ice (Fig. 9a). Due to the progressive retreat of
485 the ice body, some of these crystals are now present on the ice surface. Gypsum
486 levels comprise large single crystals (0.5-1 cm in diameter), aggregates forming
487 rafts (10 cm) up to 1 cm in thickness (Fig. 9b), as well as a fine crystalline fraction.
488 Visual examination of the fine fraction under using a binocular stereo
489 microscope indicates the presence of small aggregates of cryogenic cave
490 carbonates and gypsum (CCG) (<1 mm) including globular, single and twin
491 morphologies <1 mm in diameter (Fig. 9d).

492

493 In room G, gypsum and carbonates crystals are present in the lower part of the
494 ice deposit (Fig. 10e) and on blocks. There, CCC are larger (>10 mm) than in
495 room D and include globular shapes and raft-like aggregates, similar to those
496 reported by Žák et al. (2012). Some of these CCC show gypsum overgrowths
497 (Fig. 9f). Across the ice surface, patches of globular CCC (sub-millimetre size)
498 have been released by ice sublimation (Figs. 7a, b). In room SPD, CCC and CCG
499 (≤ 2 mm) are present within and on the ice (Figs. 2b, 7c). Finally, in room K, only
500 few CCC were still present within the ice, while most of them form heaps of loose
501 crystals covering blocks. Some of these CCCs exceed 5 mm in diameter. Crystal
502 morphologies include rosettes, skeletons and rhombohedrons similar to those
503 reported by Žák et al. (2012) as well as white tapered crystal aggregates. Beyond
504 room K, regular carbonate speleothems (i.e. stalagmites, stalactites and
505 flowstones) are present. On the contrary, gypsum crystals growing coating from
506 walls or ceilings were not observed.

507 4.5 Cave water chemistry and sulfate isotopic composition

Comentado [M26]: Reviewer #2
I452: (T, American English spelling) millilitre

Comentado [M27]: Reviewer #2
I453: (T) in room SPD, CCC and CCG

Comentado [M28]: Reviewer #2
I456: for the sake of consistency, I would drop the s at the end of CCC here.

Comentado [M29]: Sentence added:
On the contrary, Gypsum coating walls or ceilings was not observed.

508 The chemical composition of water in Devaux ~~cave (n=22) cave~~ is dominated by
509 calcium and bicarbonate with relatively high Mg concentrations and locally also
510 elevated sulfate concentrations (Table 1). Total dissolved solids (TDS, n=7) vary
511 from 57 to 315 mg l⁻¹. Devaux's dripwater has higher mean sulfate concentrations
512 (65 mg l⁻¹) than the cave river (11 mg l⁻¹) and massive and seasonal ice (2.8-18
513 mg l⁻¹). ~~Concerning the sulfur isotopic composition (Table 2), the~~ The $\delta^{34}\text{S}$ value
514 of dissolved sulfate in the dripwater is -14.4‰ (n=1), which is significantly higher
515 than in cave river water (-28.5‰ to -27.3‰, n=2; Table 2). Gypsum crystals in
516 room D show ~~homogeneous~~ $\delta^{34}\text{S}$ values ranging from -15.1‰ to -15.8‰ (n=7),
517 while in room G they range from -12.3‰ to -11.9‰ (n=5). A pyrite sample from
518 the host rock yielded a $\delta^{34}\text{S}$ value of -12.7‰ (n=1).

519 5. Discussion

520 5.1. Processes controlling the thermal regime in Devaux cave and the extent 521 current-of permafrost extent

522 A complex spatial distribution and a high degree of heterogeneity are among the
523 main characteristics of mountain permafrost (Gruber and Haeberli, 2009). In
524 Devaux cave the existence of permafrost can be related to a combination of two
525 processes: i) cave atmospheric dynamics, and ii) conductive heat transfer
526 through the rock.

527 ~~Devaux cave is characterized by mean air and rock temperatures lower than the~~
528 ~~external mean annual temperature (Fig. 5). The low cave temperatures in winter~~
529 ~~lead to an inward airflow and an associated negative thermal anomaly behind the~~
530 ~~cave entrance zone. On the contrary, during summer, the cold and dense air~~
531 ~~flows out of the cave due to the temperature difference between outside and~~
532 ~~inside air. Also, the heat supplied to the cave by the river can also~~
533 ~~modify influences the cave air temperature by exporting thermal energy. Thus,~~
534 ~~this process drags cold outside air into from the cave during winter and on the~~
535 ~~contrary during summer. Devaux cave is characterized by mean air and rock~~
536 ~~temperatures lower than the external mean annual temperature (Fig. 5). The low~~
537 ~~cave temperatures in winter lead to an inward airflow and an associated negative~~
538 ~~thermal anomaly behind the cave entrance zone.~~ Similar seasonal ventilation

Comentado [M30]: Reviewer #2

E) I315 - figure 5d, the air temperature variations at T11 and T5 (and T2) could be discussed in additional detail (at line 481 for instance).

539 patterns have been observed in ice caves elsewhere (e.g., Luetscher et al., 2008;
540 Colucci and Guglielmin, 2019; Perçoiu et al., 2021).

541 On the other hand, positive temperatures are observed both in the cave river and
542 in the air at the ~~cave~~ entrance (Fig. 5), reflecting heat advected by water (river)
543 and the influence of the external temperature (cf. Luetscher et al., 2008; Badino,
544 2010). The lack of correlation between the external and internal temperatures
545 and the small temperature variability in rooms D, G, and K reflect their thermal
546 isolation from well-ventilated cave parts. There, the apparent thermal equilibrium
547 between the rock and the cave atmosphere ($T_{\text{rock}}=T_{\text{air}}$) supports the notion that
548 heat exchange is dominated by conduction through the bedrock.

549 The MAAT at the altitude of the cave is $-0.04\text{ }^{\circ}\text{C}$ (2017-2021) suggesting that the
550 $0\text{ }^{\circ}\text{C}$ isotherm is located close to the cave. Using an array of techniques (geomatic
551 surveys, temperature monitoring, temperature at the base of the snowpack (BTS)
552 and geomorphological and thermal mapping), Serrano et al. (2019) ~~found~~
553 observed mean annual ground temperatures between -1 and $-2\text{ }^{\circ}\text{C}$ on the
554 northern slope of the MPm suggesting that discontinuous permafrost is present
555 between 2750-2900 m a.s.l., with more continuous permafrost startings at 2900
556 m a.s.l. The orientation of the Gavarnie cirque, as well as the high slope angle,
557 and shadow from the surrounding peaks favour the preservation of permafrost at
558 lower elevations (e.g., Gubler et al., 2011).

559
560 Given the high thermal inertia of the rock, the permafrost temperature at depth is
561 still under the influence of past climate conditions (e.g., Haeberli et al., 1984;
562 Noetzi and Gruber, 2009) and, therefore, part of the current permafrost in the
563 area could be inherited from previous colder times (e.g., Colucci and Guglielmin,
564 2019). In particular, the low mean annual temperatures recorded at PMBS ~~at-in~~
565 ~~the late 19th century the beginning of the Industrial Era are~~ were favourable
566 conditions for permafrost development ~~in the recent past~~. We surmise that the
567 current permafrost could be inherited from colder periods of the Little Ice Age.

568 In well-ventilated ice caves hoarfrost is the most dynamic ice formation on
569 seasonal time scales. The presence of perennial hoarfrost is, however, indicative
570 of a continuously frozen bedrock and thus representative of caves within the

Comentado [M31]: Reviewer #2
I501: (T) with more continuous permafrost starting at 2900 m asl

Comentado [M32]: Reviewer #2
D) I506-513

Comentado [M33]: Reviewer #1.
line 511: I suggest replacing the term "beginning of the Industrial Era" with "late 19th century". As far as I know the Industrial Era begun much earlier than the PMBS record.

571 permafrost zone (e.g. Luetscher and Jeannin, 2018; Yonge et al., 2018). In
572 Devaux cave, perennial hoarfrost is observed in rooms where the bedrock is
573 surrounded by small ice bodies (e.g., gallery close to SPD room, Fig. 6g). Devaux
574 (1929) indicated the presence of ice crystals on the ceiling at the entrance of
575 room D. In the same way, du Cailar and Dubois (1953) showed a schematic
576 cross-section of room D, where ice crystals are present at the beginning of the
577 room. These historical reports suggest these areas were probably more
578 ventilated in the past, which favoured the hoarfrost formation. -On the other hand,
579 seasonal hoarfrost is present in ventilated galleries (A, B, C, F and between SPD
580 and J). Seasonal hoarfrost in room B and C, and in the area between H to J,
581 disappears at the end of summer, probably because of the heat delivered by the
582 cave river, as recorded by the T5 sensor (Fig. 5).

583 The presence of permafrost in Devaux's catchment is supported by the absence
584 of drips and/or seepage in the investigated cave passages (e.g., Luetscher and
585 Jeannin, 2018; Vaks et al., 2020). Active drips and seasonal ice formations are
586 limited to the first ~15 m of the cave as well as to the inner part (beyond room K).
587 Mountain permafrost thus penetrates ~350 m longitudinally from the East-eastern
588 cliff of the Gavarnie cirque to the southern side of the massif, following a west-
589 east direction. On the other hand, given the elevation of the cave and the
590 topographic topography relief above the cave, the current maximum permafrost
591 thickness (without taking into account the active layer) on the southern side of
592 the MPm is ~200 m (without taking into account the active layer).

593

594 5.2. The origin of ice in Devaux cave

595 The transparent and massive character of Devaux's cave ice, as well as the
596 presence of CCC, which formation requires low congelation rates (Žák et al.,
597 (2004)), suggests that this ice formed by slow freezing of water dammed by ice
598 at the spring. This model is consistent with the climate in of the Gavarnie cirque,
599 cave geomorphological observations, cave air and water temperatures as well as
600 historical reports. The cave water level can rise by several meters as indicated
601 by slackwater deposits upstream of the Brulle spring.

602

Comentado [M34]: Reviewer 2:

G) I518 - the only place where perennial hoarfrost is indicated on figure 2B is a small recess appears to be surrounded by ventilated galleries containing seasonal hoarfrost, and as mentioned adjacent to a small ice body of room SPD. This certainly speaks to the frozen nature of the bedrock in this part of the cave, and demonstrates the clear effect of the negative thermal anomaly brought about by the ventilation pattern in the surrounding galleries. But if this is the case, could the authors comment on why there is no perennial hoarfrost in the galleries leading to room D, where such hoarfrost could also have developed?

Comentado [M35]:

Reviewer #2

I535-536: massive ice is formed by slow freezing - there should perhaps be a reference here.

603 The distribution and characteristics of ice bodies in Devaux cave indicate that the
604 hydraulic head rose by at least ~ 15 - 29 m, which is the elevation of the ice bodies
605 in rooms G, F and K. This situation requires that all springs (including Porche)
606 are blocked for a sufficiently long time to allow for complete freezing of these cave
607 lakes. The lack of important unconformities in this massive ice (e.g., detrital
608 layers), which are usually related to seasonal ablation (e.g., [Luetscher et al.,
609 2007; Stoffel et al., 2009; Hercman et al., 2010; Spötl et al., 2013](#)), suggests that
610 the [ice](#) deposit in room G it is the result of a single flood event. On the contrary,
611 the small unconformities recognized in the ice body in room D suggest that
612 several cycles of damming and subsequent ice formation cannot be discarded in
613 the formation of this ice deposit.

614

615 ~~Our~~ [These](#) observations indicate that under the current climate (both in the [cave](#)
616 and outside) only part of the water dammed in rooms F and E freezes during
617 winter and spring. This strongly suggests that the ice bodies in Devaux cave must
618 have been associated with colder and/or longer events of ponding and freezing
619 than today, when the cave was effectively sealed from the outside for prolonged
620 times. We hypothesize that the advance of a glacier on the steep slopes of
621 Devaux's surroundings could have contributed to the blockage of the spring,
622 leading to backflooding and the formation of large ice bodies in the cave. In the
623 study area, such periods of glacier growth occurred during the Little Ice Age
624 and/or the Neoglacial ([González Trueba et al., 2008; García-Ruiz et al., 2014,
625 2020](#)).

626

627 The freezing of a flooded cave passage cannot be explained by the advection of
628 cold air alone. It is thus surmised that heat transfer through the host rock is a
629 more plausible mechanism for the complete freezing of ~~the~~ ponded water. The
630 cave ice bodies; [just as well as](#) the presence of cryogenic [minerals](#); therefore
631 ~~represents a record of~~ a long cold period or ~~of~~ several [such shorter](#) episodes.
632 Although ~~the~~ cryogenic minerals and in particular CCC_{coarse} are typically
633 associated with permafrost thawing during warm spells ([Žák et al., 2004; Richter
634 et al., 2010; Žák et al., 2012; Luetscher et al., 2013](#)), permafrost conditions
635 prevailed during ice formation in Devaux cave. ~~Thus, the~~ water that feeds

Comentado [M36]: Reviewer #1

lines 546-552: Discordancy without visible detrital layer could also indicate unconformity. A nice example can be found in Fig5 of Hercman et al., 2010 (http://www.geochronometria.pl/pdf/geo_36/Geo36_05.pdf). This type of discordancy/unconformity could be also considered in this part of the discussion.

Comentado [M37]: Reference added:

Hercman, H., Gąsiorowski, M., Gradziński, M., and Kicińska, D.: The First Dating of Cave Ice from the Tatra Mountains, Poland and its Implication to Palaeoclimate Reconstructions, *Geochronometria*, 36, 31–38, <https://doi.org/10.2478/v10003-010-0016-2>, 2010.

Comentado [M38]: Reviewer #1:

line 554: Maybe "These" instead of "Our".

Comentado [M39]: Reviewer #2

l568: (T) The cave ice bodies [...] therefore represent

636 Devaux's springs infiltrated during late spring and summer from ponors at Lago
637 helado and/or surrounding ~~poljes, (which may have acted as local taliks).~~
638 However, the heat supplied by this water may have probably not been enough to
639 thaw the frozen host rock. It is thus very likely that the hostrock temperature was
640 ~~much~~ lower and/or the outlets remained closed ~~for~~ longer periods than today to
641 allow for the complete slow freezing of the ponded water.

Comentado [M40]: Reviewer #2:

lines 574-575: I suggest omitting the bracketed comment.

642

643 5.2.1 Ice volume changes

644 The colour changes in the walls close to the river (room E), the historical
645 photograph as well as speleological reports point to large changes (several
646 meters) ~~of in~~ the height of the seasonal ice in the flood-prone sector of the cave
647 (Figs. 8a, b). This ice is influenced by the heat exchanged between the water and
648 the cave.

649 In contrast, changes in the ice volume are almost negligible in rooms D and G
650 where the temperature is more constant and below 0°C (Figs. 7a, b). The ice
651 body in room G ~~has been retreats-retreating only~~ by only ~0.6 to ~2.2 mm a⁻¹. A
652 similar value (3 mm a⁻¹) was observed in Coulthard cave (Alberta, British
653 Columbia, [Marshall and Brown, 1974](#)), a cave located ~~with~~in permafrost ([Yonge
654 et al., 2018](#)). Changes in the ice body in this cave were related to slow sublimation
655 due to convective air flow inside the cave ([Marshall and Brown, 1974](#)). On the
656 other hand, the ice in SPD room shows higher ice retreat rates (~ 20 mm a⁻¹).
657 Similar sublimation rates have been reported in ~~others~~ ice caves in the Pamir
658 Mountains and the northern part of the Russian Platform ([Mavlyudov, 2008](#); [Žák
659 et al., 2018](#)). Overall, Devaux's cave ice deposits show a remarkable stability
660 which contrasts ~~to with~~ the rapid changes observed in ice caves outside
661 permafrost areas ([Kern and Perşoiu, 2013](#); [Perşoiu et al., 2021](#); [Wind et al.,
662 2022](#)), including other ice caves in the Pyrenees and Picos de Europa ([Belmonte-
663 Ribas et al., 2014](#); [Gomez-Lende et al., 2014, 2016](#)).

Comentado [M41]: Reviewer #2

l596: (T) which contrasts with

Con formato: Inglés (Estados Unidos)

664

665 5.3. Cryogenic cave minerals

666 In Devaux cave, CCC and CCG are still present within the ice (Figs. 6, a, b, c, d).
667 Worldwide, only very few *in situ* observations of coarse-grained cryogenic cave
668 minerals are known (e.g., [Bartolomé et al., 2015](#); [Colucci et al., 2017](#)). [du Cailar
669 and Dubois \(1953\)](#) reported the presence of gypsum crystals at ~50 cm depth
670 within the ice in Devaux cave. The first evidence of *in situ* CCC_{coarse} in cave ice
671 was reported from Sarrios 6, an ice cave at 2780 m a.s.l. on the southern slope
672 of the MPm ([Bartolomé et al., 2015](#)). [Colucci et al. \(2017\)](#) documented the
673 presence of CCC_{coarse} in a small ice cave in the Italian Alps. Recently, [Munroe et
674 al. \(2021\)](#) found CCC_{coarse} in ice of [Winter Wonderland cave](#) (Utah, USA).
675 Because of the abundance of cryogenic cave minerals, the size of individual
676 crystals and aggregates thereof, and their ~~varied-different~~ mineralogy, Devaux
677 cave provides an additional opportunity for studying the origin of such cryogenic
678 cave minerals.

679
680 ~~The~~ CCGs in Devaux cave represents, to our knowledge, the first occurrence of
681 its kind in a carbonate karst terrain. So far, CCGs ~~have~~ only been reported from
682 gypsum karst areas in Russia and Ukraine ([Korshunov and Shavrina, 1998](#); [Žák
683 et al., 2018](#) and [references therein](#)). In those ~~areascaves~~, tiny gypsum crystals
684 (~~gypsum powder~~) form during rapid freezing of water. When ice sublimates in
685 winter, ~~this~~ ~~these gypsum particles powder isare~~ released and accumulates ~~as~~
686 ~~powdery deposits~~ on the ice surface. Eventually, they ~~partly powder~~ dissolves ~~on~~
687 ~~the ice surface~~ during spring and summer due to the increase in cave air humidity,
688 and later recrystallizes forming a wide variety of ~~delicate crystal~~ morphologies.
689 CCGs from Devaux cave shows features that do not correspond to those
690 previously published from gypsum karst caves. In particular, the Devaux cave
691 CCGs i) appear together with CCC_{coarse} crystals (≥ 5 mm in some cases, in rooms
692 D and G), ii) the (raft-like) gypsum crystals are large (Fig. 9b) and, in some cases,
693 are still found within the ice (Fig. 9a) and surrounded by milky ice rich in air
694 inclusions (Fig. 9a, e), and iii) boulders are locally overgrown by gypsum (Fig.
695 9c).

696
697 Coarse-grained cryogenic cave minerals form in a semi-closed system, when ~~the~~
698 water ~~freezes very slowly~~ ~~freezes inside the caves at low freezing rates~~ ([Žák et
699 al., 2004](#)). Once supersaturation is reached, CCM start to crystallize. The

Comentado [M42]: Reviewer #2
l615: for the sake of consistency, drop s at the end of CCG
here.

700 formation of gypsum crystals requires the presence of [elevated concentrations of](#)
701 dissolved sulfate which may relate to i) sedimentary gypsum deposits intercalated
702 within carbonates (e.g., [Sancho et al., 2004](#)), ii) the presence of hydrothermal
703 water [containing](#) H₂S ~~in relation with~~ [related to](#) hydrocarbons (e.g., [Hill, 1987](#)), or
704 iii) the oxidation of sulfides (e.g., pyrite) disseminated in ~~limestones-carbonate~~
705 [rocks](#) (e.g., [Bottrell, 1991](#)). In the case of Devaux cave marine evaporite rocks
706 (e.g., of the Upper Triassic Keuper facies) and hydrocarbons are absent in the
707 catchment of the cave. The most plausible explanation for the presence of
708 dissolved sulfate in Devaux's water is the oxidation of pyrite present in the
709 limestone ([du Cailar and Dubois, 1953](#); [Requirand, 2014](#)).

Comentado [M43]: I636: (T) related to hydrocarbons

710
711 ~~Water in Devaux cave contains moderate concentrations of sulfate.~~ $\delta^{34}\text{S}$ values
712 of gypsum (-11.9 to -15.8 ‰), pyrite (-12.7 ‰), and dissolved sulfate (-14.4 ‰ in
713 dripwater and -28.5 to -27.3 ‰ in Brulle spring water) are within the range of
714 biogenic pyrite and differ notably from values of marine evaporites (10-35 ‰)
715 ([Seal, 2006](#)). Thus, the $\delta^{34}\text{S}$ values together with the geological setting of the
716 cave support the hypothesis that disseminated pyrite in the host limestone is the
717 main source of dissolved sulfate and subsequently of CCG. Only the dissolved
718 sulfate $\delta^{34}\text{S}$ values of Brulle spring are considerably more negative (-28.5‰ and
719 -27.3‰). This may be a consequence of microbially mediated redox processes
720 in the karst that discriminate against ^{34}S ([Zerkle et al., 2016](#); [Temovski et al.,](#)
721 [2018](#)). Further studies on the microbiology of the cave may shed light on these
722 mechanisms and how the local sulfur cycle may have changed in the [recent](#) past.

723
724 In gypsum caves, dissolved sulfate dominates over the bicarbonate, and the
725 typical crystallization sequence during freezing of water with high TDS is gypsum
726 → carbonate (commonly calcite) → celestine ([Žák et al., 2018](#)). In Devaux cave,
727 however, bicarbonate dominates over sulfate, and our observations show that
728 gypsum crystals partly nucleated on CCC_{coarse}. Accordingly, the crystallization
729 sequence at Devaux cave is calcite → gypsum, taking place in a semi-closed
730 system at low freezing rates.

731
732 The second aspect that makes the CCG in Devaux [cave](#) unique is the size and
733 ~~well-developed euhedral crystal~~ [shapes](#) ~~of the crystals~~ (Fig. 9 b), which differ

Comentado [M44]: I666-667: (T) is the size and well-developed shape of the crystals

734 notably from the much smaller sizes of gypsum crystals (20-200 μm) and gypsum
735 powders (1-30 μm) found in gypsum caves in Russia and Ukraine (Žák et al.,
736 2018 and references therein). Another characteristic of CCC and CCG
737 occurrences in Devaux cave is the presence of milky ice surrounding them (Fig.
738 9a, e) which seems to be related to the freezing process during the formation
739 cryogenic minerals in a subaqueous environment. Similar to that, CCC were
740 found within the ice and surrounded by bubbles in Sarríos 6 ice cave (Bartolomé
741 et al., 2015). However, the scarce presence of CCC within the ice today, together
742 with the very few sites where this topic is investigated, leads to a lack of studies
743 about gas inclusions and CO₂ degassing during CCC formation.

Comentado [M45]: Reviewer 2

H) Could the authors elaborate on why CCC or CCG related ice, rich in air inclusions could be related to the formation in a subaqueous environment?

744
745 Finally, the presence of gypsum aggregates overgrowing ~~some~~ blocks (Fig. 9c)
746 supports the hypothesis of subaqueous gypsum formation. On the other hand,
747 the absence of gypsum was never observed growing from on the ceiling or
748 on the walls, thus allowing it to discard its formation from seepage water
749 followed by precipitation due to evaporation in the cave (e.g., Gázquez et al.,
750 2017, 2020). In essence, all observations indicate that gypsum precipitated in a
751 semi-closed subaqueous environment and has been preserved from later
752 dissolution by the exceptionally dry environment of this ice cave. Gypsum
753 precipitating from freezing waters has been also documented in the Arctic and
754 the Antarctica (Losiak et al., 2016; Wollenburg et al., 2018) and has been
755 proposed as a mechanisms for gypsum formation on Mars (Losiak et al., 2016).

Comentado [M46]: Reviewer #1

lines 676-679: I think that this info could be moved forward in the section.

756 6. Conclusions

757
758 The investigation of Devaux ice cave, based on cave monitoring, geomorphology,
759 and geochemical analyses, provides exceptional insights into the origin of
760 modern and past mountain permafrost and associated processes and deposits.

761 - Devaux cave consists of two parts characterised by different thermal regimes:
762 1) the near-entrance parts and the main gallery showing large temperature
763 fluctuations and cave air temperatures seasonally exceeding 0°C. These
764 passages are influenced by ~~an~~ advective air flow and ~~the~~ heat released by the
765 cave river. 2) The inner sector and isolated chambers are characterized by
766 muted thermal oscillations and temperatures constantly below 0°C. There, the

767 cave air temperature is mainly controlled by heat conduction through the
768 bedrock.

769

770 - Devaux cave is impacted by backflooding in late winter/early spring when the
771 main outlets freeze, damming the water inside the cave forming a lake. The
772 blocking of the outlets requires temperatures below 0°C in the Gavarnie cirque,
773 while on the southern side of the Monte Perdido massif, temperatures above
774 0°C allow water infiltration.

775

776 - The absence of dripwater in most parts of the cave together with the presence
777 of perennial/seasonal hoarfrost, and the location of massive ice bodies on the
778 ceiling and/or filling cupulas and galleries are indicative of frozen bedrock
779 surrounding the cave. Permafrost at Devaux cave is attributed to a combination
780 of rock undercooling by cave air ventilation and the local climate setting giving
781 rise to the development and/or preservation of permafrost inherited from past
782 colder periods. Currently, permafrost seems to be present above the cave
783 reaching a maximum thickness of ~200 m and a lateral extension of ~350 m
784 towards the southern face of the Monte Perdido massif.

785

786 - We report the first deposits of cryogenic gypsum in a limestone-hosted ice cave.
787 Most of the cryogenic minerals are still within the ice and surrounded by milky
788 ~~ice~~ ~~ice~~ rich in air ~~inclusions~~s. Gypsum precipitation occurred subaqueously as a
789 result of slow freezing, following CCC formation. $\delta^{34}\text{S}$ values show that the
790 sulfate originated from the oxidation of pyrite present in the limestone.

791

792 - Current climate conditions seem to be still favourable for the preservation of ice
793 within this cave. This situation contrasts to the large ~~ice mass loss~~ in other ice
794 caves elsewhere. The ice deposits in Devaux ~~cave~~ allow unique insights into
795 processes leading to the formation of cryogenic carbonates and sulfates, and
796 represents ~~an ideal~~ a unique site to better understand the mountain permafrost
797 evolution in the Monte Perdido massif and the Pyrenees in general.

798 Competing interests

799 No competing of interest

Comentado [M47]: Reviewer #2:
l718: (T) rich in air inclusions

Comentado [M48]: Reviewer #1
line 723: Please consider adding "ice mass" between the word
large and loss to clarify the meaning of the sentence.

Comentado [M49]: Reviewer #2
l724: (T) in Devaux cave

800 **Authors contribution**

801 MB conceived the project, planned fieldwork and the sampling strategy. AM
802 obtained funding for this work. MB and GC installed and maintained the sensors
803 and performed the fieldwork. GC contributed with cave monitoring data from 2011
804 to 2015. MB analysed monitoring, geomorphological, and geochemical data. FG
805 performed $\delta^{34}\text{S}$ analyses using the facilities provided by AVT. JILM created the
806 radiation map. MB designed the figures and wrote a first draft of the manuscript.
807 ML and CS significantly contributed to the discussion of the data. ML and AM
808 reviewed all versions of the manuscript. All authors reviewed the manuscript and
809 contributed to the results, discussion, and final interpretation. All authors
810 approved its submission.

811 **Acknowledgements**

812 We thank the directorates of the Parc National des Pyrénées (France) and the
813 Ordesa y Monte Perdido National Park (Spain) for their permission to investigate
814 Devaux cave. We want to especially thank Marc Galy for his cave survey which
815 improves noticeably previously published surveys and for the historical photo of
816 1984. Also, we thank Météo France for providing climate data from the Pic du
817 midi de Bigorre station. We thank Maria Leunda for a critical review and
818 suggestions to the first draft of the manuscript. We also thank Jerome Labat
819 (SSPPO), Claude Novoa, Alvaro Palacios, Maria Leunda, José Leunda, David
820 Serrano, the Góriz hut staff (www.goriz.es), and the Palazio family
821 (www.hotelpalazio.com) for their invaluable help during fieldwork. We thank Paul
822 Cluzon for the photo of Fig. 1d, and Claude Requirand for his report about Devaux
823 cave. The authors would like to acknowledge the use of the Servicio General de
824 Apoyo a la Investigación-SAI, University of Zaragoza, and Alberto Barcos (IPE-
825 CSIC) for the chemical water analyses. This study contributes to the work carried
826 out by the DGA research group Procesos Geoambientales y Cambio Global (ref.:
827 E02-20R) and the MERS research group 2017 SGR 1588.

828 **Financial support**

829 This research has been supported by the following projects which were funded
830 by the National Parks Autonomous Agency (OAPN) (OCHESTRA-ref
831 2552/2020), the Spanish Agencia Estatal de Investigación (AEI-Spain)

832 (PICACHU-ref PID2019-106050RB-I00), (SPYRIT- ref CGL2016-77479-R), the
833 PaleolCE EXPLORA project (ref. CGL2015-72167-EXP) and the Comité régional
834 de spéléologie de Nouvelle Aquitaine. Miguel Bartolomé was supported by a
835 postdoctoral fellowship of the Juan de la Cierva-Formación program provided by
836 the Spanish Ministry of Science (ref.: FJCI-2017-31725) and OCHESTRA-ref
837 2552/2020. Fernando Gázquez was financially supported by a Ramón y Cajal
838 Fellowship (RYC2020-029811-I) of the Spanish Government (Ministerio de
839 Economía y Competividad).

840

841 **References**

- 842 Badino, G., 2010. UNDERGROUND METEOROLOGY-“What’s the weather underground?” Acta
843 Carsologica 39. <https://doi.org/10.3986/ac.v39i3.74>
- 844 Bartolomé, M., Sancho, C., Benito, G., Medialdea, A., Calle, M., Moreno, A., Leunda, M.,
845 Luetscher, M., Muñoz, A., Bastida, J., Cheng, H., Edwards, R.L., 2021. Effects of
846 glaciation on karst hydrology and sedimentology during the Last Glacial Cycle: The case
847 of Granito cave, Central Pyrenees (Spain). CATENA 206, 105252.
848 <https://doi.org/10.1016/j.catena.2021.105252>
- 849 Bartolomé, M., Sancho, C., Osácar, M.C., Moreno, A., Leunda, M., Spötl, C., Luetscher, M.,
850 López-Martínez, J., Belmonte, A., 2015. Characteristics of cryogenic carbonates in a
851 Pyrenean ice cave (northern Spain). Geogaceta 58 107–110.
- 852 Belmonte-Ribas, Á., Sancho, C., Moreno, A., Lopez-Martinez, J., Bartolome, M., 2014. Present-
853 day environmental dynamics in ice cave a294, central pyrenees, spain. Geogr. Fis. E
854 Din. Quat. 37, 131–140. <https://doi.org/10.4461/GFDQ.2014.37.12>
- 855 Biskaborn, B.K., Smith, S.L., Noetzi, J., Matthes, H., Vieira, G., Streletskiy, D.A., Schoeneich, P.,
856 Romanovsky, V.E., Lewkowicz, A.G., Abramov, A., Allard, M., Boike, J., Cable, W.L.,
857 Christiansen, H.H., Delaloye, R., Diekmann, B., Drozdov, D., Etzelmüller, B., Grosse, G.,
858 Guglielmin, M., Ingeman-Nielsen, T., Isaksen, K., Ishikawa, M., Johansson, M.,
859 Johannsson, H., Joo, A., Kaverin, D., Kholodov, A., Konstantinov, P., Kröger, T., Lambiel,
860 C., Lanckman, J.-P., Luo, D., Malkova, G., Meiklejohn, I., Moskalenko, N., Oliva, M.,
861 Phillips, M., Ramos, M., Sannel, A.B.K., Sergeev, D., Seybold, C., Skryabin, P., Vasiliev,
862 A., Wu, Q., Yoshikawa, K., Zheleznyak, M., Lantuit, H., 2019. Permafrost is warming at a
863 global scale. Nat. Commun. 10, 264. <https://doi.org/10.1038/s41467-018-08240-4>
- 864 Boeckli, L., Brenning, A., Gruber, S., Noetzi, J., 2012. A statistical approach to modelling
865 permafrost distribution in the European Alps or similar mountain ranges. The
866 Cryosphere 6, 125–140. <https://doi.org/10.5194/tc-6-125-2012>
- 867 Bottrell, S.H., 1991. Sulphur isotope evidence for the origin of cave evaporites in Ogof y Daren
868 Cilau, south Wales. Mineral. Mag. 55, 209–210.
869 <https://doi.org/10.1180/minmag.1991.055.379.09>
- 870 Bücher, A., Dessens, J., 1991. Secular Trend of Surface Temperature at an Elevated
871 Observatory in the Pyrenees. J. Clim. 4, 859–868. [https://doi.org/10.1175/1520-0442\(1991\)004<0859:STOSTA>2.0.CO;2](https://doi.org/10.1175/1520-0442(1991)004<0859:STOSTA>2.0.CO;2)
- 872 Casteret, N., 1953. Dans les glaces souterraines. Les plus élevés de Monde. Libraire
873 Académique Perrin, Paris, p. 93.

875 Colucci, R., Luetscher, M., Fortee, E., Guglielmin, M., Lenaz, D., Princivalle, F., Vita, F., 2017.
876 First alpine evidence of in situ coarse cryogenic cave carbonates (CCCcoarse). *Geogr.*
877 *Fis. E Din. Quat.* 53–59. <https://doi.org/10.4461/GFDQ.2017.40.5>

878 Colucci, R.R., Guglielmin, M., 2019. Climate change and rapid ice melt: Suggestions from abrupt
879 permafrost degradation and ice melting in an alpine ice cave. *Prog. Phys. Geogr. Earth*
880 *Environ.* 0309133319846056. <https://doi.org/10.1177/0309133319846056>

881 Dessens, J., Bücher, A., 1995. Changes in minimum and maximum temperatures at the Pic du
882 Midi in relation with humidity and cloudiness, 1882–1984. *Atmospheric Res., Minimax*
883 *Workshop* 37, 147–162. [https://doi.org/10.1016/0169-8095\(94\)00075-0](https://doi.org/10.1016/0169-8095(94)00075-0)

884 Devaux, J., 1929. Nouvelle grotte Marboréenne. *La Natura* 102–107.

885 [Devaux, J., 1933. La grotte des sœurs de la cascade. Études glaciologiques, 1920-1930. Tome](#)
886 [VII, pp. 233-238. Plan & coupe. Paris. Imprimerie Nationale. Ministère de l'Agriculture.](#)
887 [Direction des eaux et du génie rural.](#)

888 du Cailar, J., Couderc, J., Dubois, P., 1953. La source du Gave de Pau. *Annales de Spéléologie*
889 181–203.

890 du Cailar, J., Dubois, P., 1953. Sur quelques modalités de formation et d'évolution des dépôts
891 cristallins dans les cavités de haute altitude. In: Premier congrès international de
892 spéléologie. Paris, Tome II, pp 325-333.

893 Dublyansky, Y., Moseley, G.E., Lyakhnitsky, Y., Cheng, H., Edwards, L.R., Scholz, D., Koltai, G.,
894 Spötl, C., 2018. Late Palaeolithic cave art and permafrost in the Southern Ural. *Sci. Rep.*
895 8, 12080. <https://doi.org/10.1038/s41598-018-30049-w>

896 Fankhauser, A., McDermott, F., Fleitmann, D., 2016. Episodic speleothem deposition tracks the
897 terrestrial impact of millennial-scale last glacial climate variability in SW Ireland. *Quat.*
898 *Sci. Rev.* 152, 104–117. <https://doi.org/10.1016/j.quascirev.2016.09.019>

899 Feuillet, T., 2011. Statistical Analyses of Active Patterned Ground Occurrence in the Taillon
900 Massif (Pyrénées, France/Spain). *Permafr. Periglac. Process.* 22, 228–238.
901 <https://doi.org/10.1002/ppp.726>

902 García-Ruiz, J.M., Palacios, D., Andrés, N. de, Valero-Garcés, B.L., López-Moreno, J.I., Sanjuán,
903 Y., 2014. Holocene and 'Little Ice Age' glacial activity in the Marboré Cirque, Monte
904 Perdido Massif, Central Spanish Pyrenees. *The Holocene* 24, 1439–1452.
905 <https://doi.org/10.1177/0959683614544053>

906 García-Ruiz, J.M., Palacios, D., Andrés, N., López-Moreno, J.I., 2020. Neoglaciation in the
907 Spanish Pyrenees: a multiproxy challenge. *Mediterr. Geosci. Rev.* 2, 21–36.
908 <https://doi.org/10.1007/s42990-020-00022-9>

909 Gázquez, F., Bauska, T.K., Comas-Bru, L., Ghaleb, B., Calaforra, J.-M., Hodell, D.A., 2020. The
910 potential of gypsum speleothems for paleoclimatology: application to the Iberian
911 Roman Humid Period. *Sci. Rep.* 10, 14705. [https://doi.org/10.1038/s41598-020-71679-](https://doi.org/10.1038/s41598-020-71679-3)
912 3

913 Gázquez, F., Calaforra, J.M., Evans, N.P., Hodell, D.A., 2017. Using stable isotopes ($\delta^{17}\text{O}$, $\delta^{18}\text{O}$
914 and δD) of gypsum hydration water to ascertain the role of water condensation in the
915 formation of subaerial gypsum speleothems. *Chem. Geol.* 452, 34–46.
916 <https://doi.org/10.1016/j.chemgeo.2017.01.021>

917 Gellatly, A.F., Grove, J.M., Switsur, V.R., 1992. Mid-Holocene glacial activity in the Pyrenees.
918 *The Holocene* 2, 266–270. <https://doi.org/10.1177/095968369200200309>

919 Giesemann, A., Jaeger, H.-J., Norman, A.L., Krouse, H.R., Brand, W.A., 1994. Online Sulfur-
920 Isotope Determination Using an Elemental Analyzer Coupled to a Mass Spectrometer.
921 *Anal. Chem.* 66, 2816–2819. <https://doi.org/10.1021/ac00090a005>

922 Gomez Lende, M., Berenguer, F., Serrano, E., 2014. Morphology, ice types and thermal regime
923 in a high mountain ice cave. First studies applying terrestrial laser scanner in the *Papeña*

924 [Ceastil ice cave \(Picos de Europa, Northern Spain\). Geogr. Fis. E Din. Quat. 37, 141–150.](https://doi.org/10.4461/GFDQ.2014.37.13)
925 <https://doi.org/10.4461/GFDQ.2014.37.13>
926 Gómez Lende, M., Serrano, E., Bordehore, L.J., Sandoval, S., 2016. The role of GPR techniques
927 in determining ice cave properties: Peña Castil ice cave, Picos de Europa. *Earth Surf.*
928 *Process. Landf.* 41, 2177–2190. <https://doi.org/10.1002/esp.3976>
929 Gómez-Ortiz, A., Oliva, M., Salvador-Franch, F., Palacios, D., Tanarro, L.M., de Sanjosé-Blasco,
930 J.J., Salvà-Catarineu, M., 2019. Monitoring permafrost and periglacial processes in
931 Sierra Nevada (Spain) from 2001 to 2016. *Permafr. Periglac. Process.* 30, 278–291.
932 <https://doi.org/10.1002/ppp.2002>
933 González Trueba, J.J., Moreno, R.M., Martínez de Pisón, E., Serrano, E., 2008. ‘Little Ice Age’
934 glaciation and current glaciers in the Iberian Peninsula. *The Holocene* 18, 551–568.
935 <https://doi.org/10.1177/0959683608089209>
936 Gruber, S., Haeberli, W., 2009. Mountain Permafrost, in: Margesin, R. (Ed.), *Permafrost Soils,*
937 *Soil Biology.* Springer, Berlin, Heidelberg, pp. 33–44. [https://doi.org/10.1007/978-3-](https://doi.org/10.1007/978-3-540-69371-0_3)
938 [540-69371-0_3](https://doi.org/10.1007/978-3-540-69371-0_3)
939 Gubler, S., Fiddes, J., Keller, M., Gruber, S., 2011. Scale-dependent measurement and analysis
940 of ground surface temperature variability in alpine terrain. *The Cryosphere* 5, 431–443.
941 <https://doi.org/10.5194/tc-5-431-2011>
942 Haeberli, W., Rellstab, W., Harrison, W.D., 1984. Geothermal Effects of 18 ka BP Ice Conditions
943 in the Swiss Plateau. *Ann. Glaciol.* 5, 56–60. [https://doi.org/10.3189/1984AoG5-1-56-](https://doi.org/10.3189/1984AoG5-1-56-60)
944 [60](https://doi.org/10.3189/1984AoG5-1-56-60)
945 Harris, C., Vonder Mühl, D., Isaksen, K., Haeberli, W., Sollid, J.L., King, L., Holmlund, P., Dramis,
946 F., Guglielmin, M., Palacios, D., 2003. Warming permafrost in European mountains.
947 *Glob. Planet. Change* 39, 215–225. <https://doi.org/10.1016/j.gloplacha.2003.04.001>
948 Heeb, B., 2014. The Next Generation of the DistoX Cave Surveying Instrument. *CREG J.*, 88, 5–8.
949 Hercman, H., Gaşiorowski, M., Gradziński, M., Kicińska, D., 2010. The First Dating of Cave Ice
950 from the Tatra Mountains, Poland and its Implication to Palaeoclimate
951 Reconstructions. *Geochronometria* 36, 31–38. [https://doi.org/10.2478/v10003-010-](https://doi.org/10.2478/v10003-010-0016-2)
952 [0016-2](https://doi.org/10.2478/v10003-010-0016-2)
953 Hill, C.A., 1987. Geology of Carlsbad Cavern and other caves in the Guadalupe Mountains, New
954 Mexico and Texas. *Bull 117 N. M. Bur. Mines Miner. Resour.*
955 Hock, R., Rasul, G., Adler, C., Cáceres, B., Gruber, S., Hirabayashi, Y., Jackson, J., Käab, A., Kang,
956 S., Kutuzov, S., Milner, A., Molau, U., Morin, S., Orlove, B., Steltzer, H., 2019. High
957 Mountain Areas. In: *IPCC Special Report on the Ocean and Cryosphere in a Changing*
958 *Climate.*
959 Kern, Z., Bočić, N., Sipos, G., 2018. Radiocarbon-Dated Vegetal Remains from the Cave Ice
960 Deposits of Velebit Mountain, Croatia. *Radiocarbon* 60, 1391–1402.
961 <https://doi.org/10.1017/RDC.2018.108>
962 Kern, Z., Perşoiu, A., 2013. Cave ice – the imminent loss of untapped mid-latitude cryospheric
963 palaeoenvironmental archives. *Quat. Sci. Rev.* 67, 1–7.
964 <https://doi.org/10.1016/j.quascirev.2013.01.008>
965 Koltai, G., Spötl, C., Cheng, H., 2020. Cryogenic cave carbonates in the Dolomites (Northern
966 Italy): insights into Younger Dryas cooling and seasonal precipitation. *Clim. Past*
967 *Discuss.* 1–25. <https://doi.org/10.5194/cp-2020-107>
968 Korshunov, V.V., Shavrina, E.V., 1998. Gypsum speleothems of freezing origin. *J. Cave Karst*
969 *Stud.* 60, 146–150.
970 Lechleitner, F.A., Mason, A.J., Breitenbach, S.F.M., Vaks, A., Haghypour, N., Henderson, G.M.,
971 2020. Permafrost-related hiatuses in stalagmites: Evaluating the potential for
972 reconstruction of carbon cycle dynamics. *Quat. Geochronol.* 56, 101037.
973 <https://doi.org/10.1016/j.quageo.2019.101037>
974 Leunda, M., González-Sampériz, P., Gil-Romera, G., Bartolomé, M., Belmonte-Ribas, Á., Gómez-
975 García, D., Kaltenrieder, P., Rubiales, J.M., Schwörer, C., Tinner, W., Morales-Molino,

976 C., Sancho, C., 2019. Ice cave reveals environmental forcing of long-term Pyrenean tree
977 line dynamics. *J. Ecol.* 107, 814–828. <https://doi.org/10.1111/1365-2745.13077>

978 Lewkowicz, A.G., Ednie, M., 2004. Probability mapping of mountain permafrost using the BTS
979 method, Wolf Creek, Yukon Territory, Canada. *Permafr. Periglac. Process.* 15, 67–80.
980 <https://doi.org/10.1002/ppp.480>

981 Li, T.-Y., Baker, J.L., Wang, T., Zhang, J., Wu, Y., Li, H.-C., Blyakharchuk, T., Yu, T.-L., Shen, C.-C.,
982 Cheng, H., Kong, X.-G., Xie, W.-L., Edwards, R.L., 2021. Early Holocene permafrost
983 retreat in West Siberia amplified by reorganization of westerly wind systems.
984 *Commun. Earth Environ.* 2, 1–11. <https://doi.org/10.1038/s43247-021-00238-z>

985 López-Moreno, J.I., Alonso-González, E., Monserrat, O., Del Río, L.M., Otero, J., Lapazaran, J.,
986 Luzi, G., Dematteis, N., Serreta, A., Rico, I., Serrano-Cañadas, E., Bartolomé, M.,
987 Moreno, A., Buisan, S., Revuelto, J., 2019. Ground-based remote-sensing techniques
988 for diagnosis of the current state and recent evolution of the Monte Perdido Glacier,
989 Spanish Pyrenees. *J. Glaciol.* 65, 85–100. <https://doi.org/10.1017/jog.2018.96>

990 López-Moreno, J.I., Revuelto, J., Rico, I., Chueca-Cía, J., Julián, A., Serreta, A., Serrano, E.,
991 Vicente-Serrano, S.M., Azorin-Molina, C., Alonso-González, E., García-Ruiz, J.M., 2016.
992 Thinning of the Monte Perdido Glacier in the Spanish Pyrenees since 1981. *The*
993 *Cryosphere* 10, 681–694. <https://doi.org/10.5194/tc-10-681-2016>

994 Losiak, A., Derkowski, A., Skała, A., Trzciński, J., 2016. Evaporites on ice: how to form gypsum
995 on Antarctica and on Martian North polar residual cap? In: 47th Lunar and Planetary
996 Science Conference. 1972.pdf.

997 Luetscher, M., Bolius, D., Schwikowski, M., Schotterer, U., Smart, P.L., 2007. Comparison of
998 techniques for dating of subsurface ice from Monlesi ice cave, Switzerland. *J. Glaciol.*
999 53, 374–384.

1000 Luetscher, M., Borreguero, M., Moseley, G.E., Spötl, C., Edwards, R.L., 2013. Alpine permafrost
1001 thawing during the Medieval Warm Period identified from cryogenic cave carbonates.
1002 *The Cryosphere* 7, 1073–1081. <https://doi.org/10.5194/tc-7-1073-2013>

1003 Luetscher, M., Jeannin, P.-Y., 2018. Chapter 12 - Ice Caves in Switzerland, in: Perçoiu, A.,
1004 Lauritzen, S.-E. (Eds.), *Ice Caves*. Elsevier, pp. 221–235. <https://doi.org/10.1016/B978-0-12-811739-2.00010-3>

1006 Luetscher, M., Lismonde, B., Jeannin, P.-Y., 2008. Heat exchanges in the heterothermic zone of
1007 a karst system: Monlesi cave, Swiss Jura Mountains. *J. Geophys. Res. Earth Surf.* 113.
1008 <https://doi.org/10.1029/2007JF000892>

1009 Lundberg, J., McFarlane, D.A., 2007. Pleistocene depositional history in a periglacial terrane: A
1010 500 k.y. record from Kents Cavern, Devon, United Kingdom. *Geosphere* 3, 199–219.
1011 <https://doi.org/10.1130/GES00085.1>

1012 Marshall, P., Brown, M.C., 1974. Ice in Coulthard Cave, Alberta. *Can. J. Earth Sci.*
1013 <https://doi.org/10.1139/e74-045>

1014 Mavlyudov, B.R., 2008. Caves Glaciation in the Past. Федеральное государственное
1015 бюджетное учреждение науки Институт географии Российской академии наук, pp.
1016 499–505.

1017 Moseley, G.E., Edwards, R.L., Lord, N.S., Spötl, C., Cheng, H., 2021. Speleothem record of mild
1018 and wet mid-Pleistocene climate in northeast Greenland. *Sci. Adv.* 7, eabe1260.
1019 <https://doi.org/10.1126/sciadv.abe1260>

1020 Munroe, J., Kimble, K., Spötl, C., Marks, G.S., McGee, D., Herron, D., 2021. Cryogenic cave
1021 carbonate and implications for thawing permafrost at Winter Wonderland Cave, Utah,
1022 USA. *Sci. Rep.* 11, 6430. <https://doi.org/10.1038/s41598-021-85658-9>

1023 Munroe, J.S., 2021. First investigation of perennial ice in Winter Wonderland Cave, Uinta
1024 Mountains, Utah, USA. *The Cryosphere* 15, 863–881. <https://doi.org/10.5194/tc-15-863-2021>

1026 Navarro-Serrano, F., López-Moreno, J.I., Azorin-Molina, C., Alonso-González, E., Tomás-
1027 Burguera, M., Sanmiguel-Vallelado, A., Revuelto, J., Vicente-Serrano, S.M., 2018.

1028 Estimation of near-surface air temperature lapse rates over continental Spain and its
1029 mountain areas. *Int. J. Climatol.* 38, 3233–3249. <https://doi.org/10.1002/joc.5497>
1030 Noetzi, J., Gruber, S., 2009. Transient thermal effects in Alpine permafrost. *The Cryosphere* 3,
1031 85–99. <https://doi.org/10.5194/tc-3-85-2009>
1032 Orvošová, M., Deininger, M., Milovský, R., 2014. Permafrost occurrence during the Last
1033 Permafrost Maximum in the Western Carpathian Mountains of Slovakia as inferred
1034 from cryogenic cave carbonate. *Boreas* 43, 750–758.
1035 <https://doi.org/10.1111/bor.12042>
1036 Perşoiu, A., Buzjak, N., Onaca, A., Pennos, C., Sotiriadis, Y., Ionita, M., Zachariadis, S., Styllas,
1037 M., Kosutnik, J., Hegyi, A., Butorac, V., 2021. Record summer rains in 2019 led to
1038 massive loss of surface and cave ice in SE Europe. *The Cryosphere* 15, 2383–2399.
1039 <https://doi.org/10.5194/tc-15-2383-2021>
1040 Perşoiu, A., Lauritzen, S.-E. (Eds.), 2018. *Ice caves*. Elsevier, Amsterdam, Netherlands.
1041 Perşoiu, A., Onac, B.P., Wynn, J.G., Blaauw, M., Ionita, M., Hansson, M., 2017. Holocene winter
1042 climate variability in Central and Eastern Europe. *Sci. Rep.* 7, 1196.
1043 <https://doi.org/10.1038/s41598-017-01397-w>
1044 Pons, X., Ninyerola, M., 2008. Mapping a topographic global solar radiation model
1045 implemented in a GIS and refined with ground data. *Int. J. Climatol.* 28, 1821–1834.
1046 <https://doi.org/10.1002/joc.1676>
1047 Racine, T.M.F., Spötl, C., Reimer, P.J., Čarga, J., 2022. RADIOCARBON CONSTRAINTS ON
1048 PERIODS OF POSITIVE CAVE ICE MASS BALANCE DURING THE LAST MILLENNIUM,
1049 JULIAN ALPS (NW SLOVENIA). *Radiocarbon* 1–24.
1050 <https://doi.org/10.1017/RDC.2022.26>
1051 Reille, M., Andrieu, V., 1995. The late Pleistocene and Holocene in the Lourdes Basin, Western
1052 Pyrénées, France: new pollen analytical and chronological data. *Veg. Hist.*
1053 *Archaeobotany* 4, 1–21. <https://doi.org/10.1007/BF00198611>
1054 Requirand, C., 2014. Hypothèse sur la formation des cristaux de gypse Grotte Glacée Devaux
1055 (Gavarnie - Hautes Pyrénées). *Bulletin de la Société Ramon.* 11 pp.
1056 Richter, D.K., Meissner, P., Immenhauser, A., Schulte, U., Dorsten, I., 2010a. Cryogenic and
1057 non-cryogenic pool calcites indicating permafrost and non-permafrost periods: a case
1058 study from the Herbslabyrinth-Advent Cave system (Germany). *The Cryosphere* 4,
1059 501–509. <https://doi.org/10.5194/tc-4-501-2010>
1060 Richter, D.K., Meissner, P., Immenhauser, A., Schulte, U., Dorsten, I., 2010b. Cryogenic and
1061 non-cryogenic pool calcites indicating permafrost and non-permafrost periods: a case
1062 study from the Herbslabyrinth-Advent Cave system (Germany). *The Cryosphere* 4,
1063 501–509. <https://doi.org/10.5194/tc-4-501-2010>
1064 Rico, I., Magnin, F., López Moreno, J.I., Serrano, E., Alonso-González, E., Revuelto, J., Hughes-
1065 Allen, L., Gómez-Lende, M., 2021. First evidence of rock wall permafrost in the
1066 Pyrenees (Vignemale peak, 3,298 m a.s.l., 42°46'16"N/0°08'33"W). *Permafr. Periglac.*
1067 *Process.* 32, 673–680. <https://doi.org/10.1002/ppp.2130>
1068 Rodríguez-Salgado, P., Oms, O., Ibáñez-Insa, J., Anadón, P., Gómez de Soler, B., Campeny, G.,
1069 Agustí, J., 2021. Mineralogical proxies of a Pliocene maar lake recording changes in
1070 precipitation at the Camp dels Ninots (Pliocene, NE Iberia). *Sediment. Geol.* 418,
1071 105910. <https://doi.org/10.1016/j.sedgeo.2021.105910>
1072 Rösch, G., Rösch, J., 1935. Visites à la grotte Devaux. *La Montagne. Revue du Club Alpin*
1073 *Français*, N° 269, pp.171-178.
1074 Rösch, J., 1949. Une exploration de la Grotte Devaux à Gavarnie. *Bulletin de la section du Sud-*
1075 *Ouest de la Club Alpin Français*, N°69. pp. 103-107.
1076 Sancho, C., Arenas, C., Pardo, G., Peña-Monné, J.L., Rhodes, E.J., Bartolomé, M., García-Ruiz,
1077 J.M., Martí-Bono, C., 2018a. Glaciolacustrine deposits formed in an ice-dammed
1078 tributary valley in the south-central Pyrenees: New evidence for late Pleistocene
1079 climate. *Sediment. Geol.* 366, 47–66. <https://doi.org/10.1016/j.sedgeo.2018.01.008>

- 1080 Sancho, C., Belmonte, Á., Bartolomé, M., Moreno, A., Leunda, M., López-Martínez, J., 2018b.
1081 Middle-to-late Holocene palaeoenvironmental reconstruction from the A294 ice-cave
1082 record (Central Pyrenees, northern Spain). *Earth Planet. Sci. Lett.* 484, 135–144.
1083 <https://doi.org/10.1016/j.epsl.2017.12.027>
- 1084 Sancho, C., Peña, J.L., Mikkan, R., Osácar, C., Quinif, Y., 2004. Morphological and speleothemic
1085 development in Brujas Cave (Southern Andean Range, Argentine):
1086 palaeoenvironmental significance. *Geomorphology* 57, 367–384.
1087 [https://doi.org/10.1016/S0169-555X\(03\)00166-1](https://doi.org/10.1016/S0169-555X(03)00166-1)
- 1088 Scandroglio, R., Draebing, D., Offer, M., Krautblatter, M., 2021. 4D quantification of alpine
1089 permafrost degradation in steep rock walls using a laboratory-calibrated electrical
1090 resistivity tomography approach. *Surf. Geophys.* 19, 241–260.
1091 <https://doi.org/10.1002/nsg.12149>
- 1092 Seal, R.R., II, 2006. Sulfur Isotope Geochemistry of Sulfide Minerals. *Rev. Mineral. Geochem.*
1093 61, 633–677. <https://doi.org/10.2138/rmg.2006.61.12>
- 1094 Serrano, E., Gómez-Lende, M., Belmonte, Á., Sancho, C., Sánchez-Benítez, J., Bartolomé, M.,
1095 Leunda, M., Moreno, A., Hivert, B., 2018. Chapter 28 - Ice Caves in Spain, in: Perşoiu,
1096 A., Lauritzen, S.-E. (Eds.), *Ice Caves*. Elsevier, pp. 625–655.
1097 <https://doi.org/10.1016/B978-0-12-811739-2.00028-0>
- 1098 Serrano, E., López-Moreno, J.I., Gómez-Lende, M., Pisabarro, A., Martín-Moreno, R., Rico, I.,
1099 Alonso-González, E., 2020. Frozen ground and periglacial processes relationship in
1100 temperate high mountains: a case study at Monte Perdido-Tucarroya area (The
1101 Pyrenees, Spain). *J. Mt. Sci.* 17, 1013–1031. [https://doi.org/10.1007/s11629-019-5614-](https://doi.org/10.1007/s11629-019-5614-5)
1102 5
- 1103 Serrano, E., Sanjosé-Blasco, J.J. de, Gómez-Lende, M., López-Moreno, J.I., Pisabarro, A.,
1104 Martínez-Fernández, A., 2019. Periglacial environments and frozen ground in the
1105 central Pyrenean high mountain area: Ground thermal regime and distribution of
1106 landforms and processes. *Permafr. Periglac. Process.* 30, 292–309.
1107 <https://doi.org/10.1002/ppp.2032>
- 1108 Spötl, C., Cheng, H., 2014. Holocene climate change, permafrost and cryogenic carbonate
1109 formation: insights from a recently deglaciated, high-elevation cave in the Austrian
1110 Alps. *Clim. Past* 10, 1349–1362. <https://doi.org/10.5194/cp-10-1349-2014>
- 1111 Spötl, C., Koltai, G., Jarosch, A.H., Cheng, H., 2021. Increased autumn and winter precipitation
1112 during the Last Glacial Maximum in the European Alps. *Nat. Commun.* 12, 1839.
1113 <https://doi.org/10.1038/s41467-021-22090-7>
- 1114 Spötl, C., Reimer, P.J., Luetscher, M., 2014. Long-term mass balance of perennial firn and ice
1115 in an Alpine cave (Austria): Constraints from radiocarbon-dated wood fragments. *The*
1116 *Holocene* 0959683613515729. <https://doi.org/10.1177/0959683613515729>
- 1117 Stoffel, M., Luetscher, M., Bollschweiler, M., Schlatter, F., 2009. Evidence of NAO control on
1118 subsurface ice accumulation in a 1200 yr old cave-ice sequence, St. Livres ice cave,
1119 Switzerland. *Quat. Res.* 72, 16–26. <https://doi.org/10.1016/j.yqres.2009.03.002>
- 1120 Supper, R., Ottowitz, D., Jochum, B., Römer, A., Pfeiler, S., Kauer, S., Keuschnig, M., Ita, A.,
1121 2014. Geoelectrical monitoring of frozen ground and permafrost in alpine areas: field
1122 studies and considerations towards an improved measuring technology. *Surf. Geophys.*
1123 12, 93–115. <https://doi.org/10.3997/1873-0604.2013057>
- 1124 Temovski, M., Futó, I., Túri, M., Palcsu, L., 2018. Sulfur and oxygen isotopes in the gypsum
1125 deposits of the Provalata sulfuric acid cave (Macedonia). *Geomorphology* 315, 80–90.
1126 <https://doi.org/10.1016/j.geomorph.2018.05.010>
- 1127 Vaks, A., Gutareva, O.S., Breitenbach, S.F.M., Avirmed, E., Mason, A.J., Thomas, A.L., Osinzev,
1128 A.V., Kononov, A.M., Henderson, G.M., 2013. Speleothems Reveal 500,000-Year
1129 History of Siberian Permafrost. *Science* 340, 183–186.
1130 <https://doi.org/10.1126/science.1228729>

- 1131 Vaks, A., Mason, A.J., Breitenbach, S.F.M., Kononov, A.M., Osinzev, A.V., Rosensaft, M.,
 1132 Borshevsky, A., Gutareva, O.S., Henderson, G.M., 2020. Palaeoclimate evidence of
 1133 vulnerable permafrost during times of low sea ice. *Nature* 577, 221–225.
 1134 <https://doi.org/10.1038/s41586-019-1880-1>
- 1135 Wind, M., Obleitner, F., Racine, T., Spötl, C., 2022. Multi-annual temperature evolution and
 1136 implications for cave ice development in a sag-type ice cave in the Austrian Alps.
 1137 *Cryosphere Discuss.* 1–26. <https://doi.org/10.5194/tc-2022-67>
- 1138 Wollenburg, J.E., Katlein, C., Nehrke, G., Nöthig, E.-M., Matthiessen, J., Wolf- Gladrow, D.A.,
 1139 Nikolopoulos, A., Gázquez-Sanchez, F., Rossmann, L., Assmy, P., Babin, M., Bruyant, F.,
 1140 Beaulieu, M., Dybwad, C., Peeken, I., 2018. Ballasting by cryogenic gypsum enhances
 1141 carbon export in a Phaeocystis under-ice bloom. *Sci. Rep.* 8, 7703.
 1142 <https://doi.org/10.1038/s41598-018-26016-0>
- 1143 Yonge, C.J., Ford, D., Horne, G., Lauriol, B., Schroeder, J., 2018. Chapter 15 - Ice Caves in
 1144 Canada, in: Perşoiu, A., Lauritzen, S.-E. (Eds.), *Ice Caves*. Elsevier, pp. 285–334.
 1145 <https://doi.org/10.1016/B978-0-12-811739-2.00015-2>
- 1146 Žák, K., Onac, B.P., Kadebskaya, O.I., Filippi, M., Dublyansky, Y., Luetscher, M., 2018. Chapter 6
 1147 - Cryogenic Mineral Formation in Caves, in: Perşoiu, A., Lauritzen, S.-E. (Eds.), *Ice*
 1148 *Caves*. Elsevier, pp. 123–162. <https://doi.org/10.1016/B978-0-12-811739-2.00035-8>
- 1149 Žák, K., Richter, D.K., Filippi, M., Živor, R., Deininger, M., Mangini, A., Scholz, D., 2012. Coarsely
 1150 crystalline cryogenic cave carbonate – a new archive to estimate the Last
 1151 Glacial minimum permafrost depth in Central Europe. *Clim. Past* 8, 1821–1837.
 1152 <https://doi.org/10.5194/cp-8-1821-2012>
- 1153 Žák, K., Urban, J., Cílek, V., Hercman, H., 2004. Cryogenic cave calcite from several Central
 1154 European caves: age, carbon and oxygen isotopes and a genetic model. *Chem. Geol.*
 1155 206, 119–136. <https://doi.org/10.1016/j.chemgeo.2004.01.012>
- 1156 Zerkle, A.L., Jones, D.S., Farquhar, J., Macalady, J.L., 2016. Sulfur isotope values in the sulfidic
 1157 Frasassi cave system, central Italy: A case study of a chemolithotrophic S-based
 1158 ecosystem. *Geochim. Cosmochim. Acta* 173, 373–386.
 1159 <https://doi.org/10.1016/j.gca.2015.10.028>

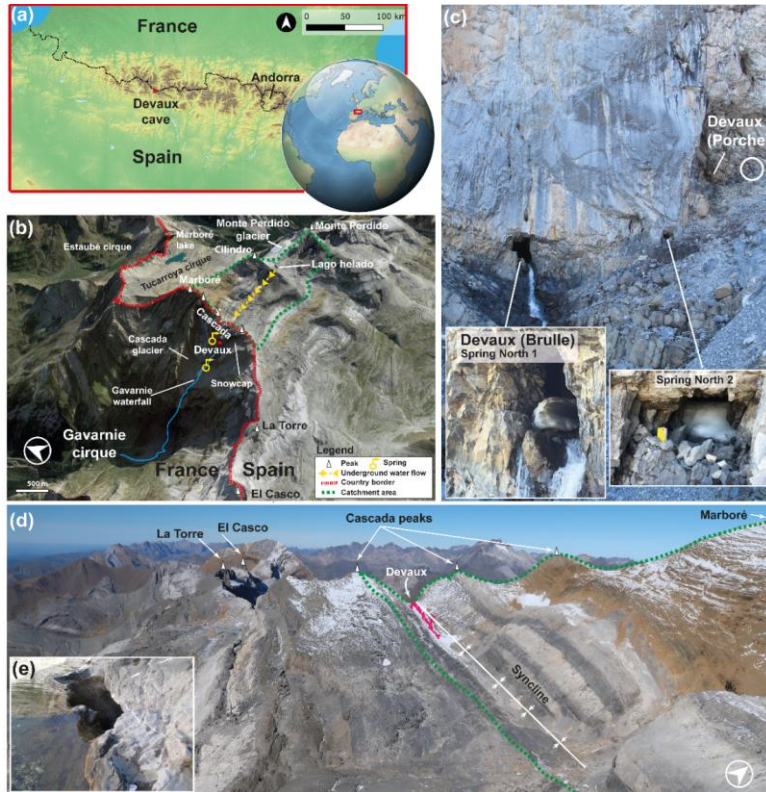


Figure 1. (a) Location of Devaux cave in the Central Pyrenees (ASTER GDEM, NASA v3, 2019). (b) Satellite image and location of Devaux cave, main peaks, lakes, glaciers and cirques in the study area (3D ©Google Earth). The yellow arrows indicate the underground flow path from Lago helado to the Gavarnie waterfall according to the dye-tracing experiment of [du Cailar et al. \(1953\)](#). (c) View towards the entrances of Devaux cave. The lower entrance (~2821 m a.s.l.) corresponds to the Brulle spring (Spring North 1), while the upper one corresponds to the main entrance (Porche (South), ~2836 m a.s.l.). Spring North 2 is located between both entrances. Note person for scale (within the white circle). Remnants of ice partially blocking Brulle and Spring North 2 (July 2021). (d) Landscape view of the catchment area and approximate location of Devaux cave (in dark pink; photo: Paul Cluzon). (e) Ponor located on the southern shore of Lago Helado.

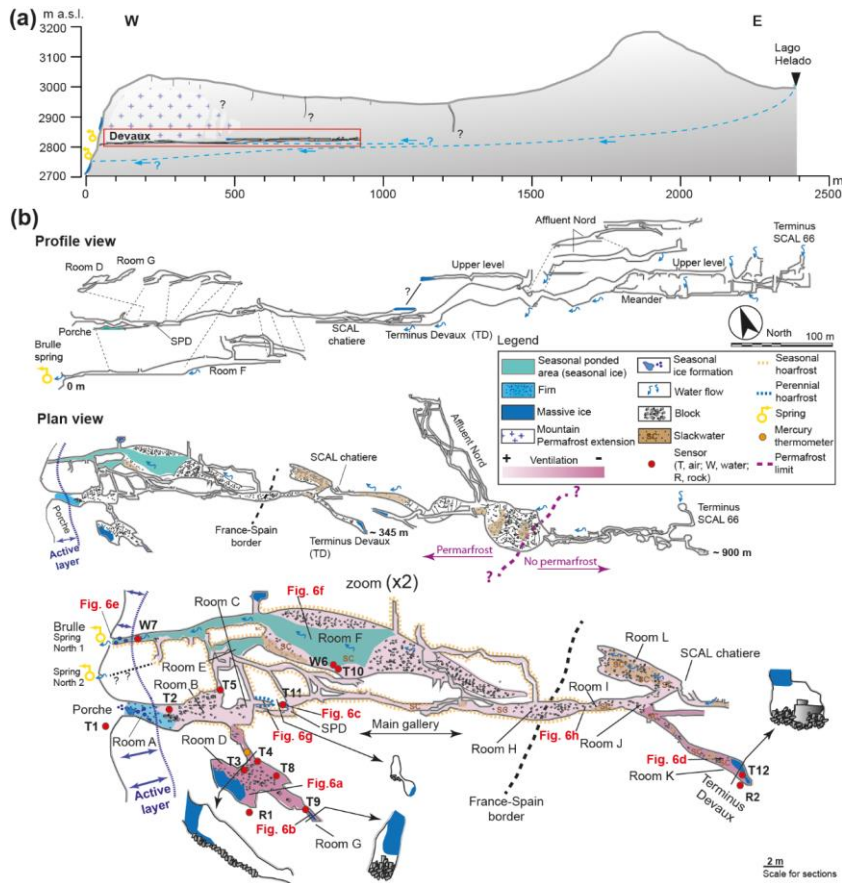


Figure 2. (a) Schematic W-E cross section from Lago helado to Devaux cave, the assumed extent of mountain permafrost, and ~~and~~ the interpreted underground flow path according to du Cailar et al. (1953). (b) Longitudinal section and plan view of Devaux cave showing the locations of sensors and cave deposits. Labels R, W and T refer to rock, water and air temperature sensors, respectively. The enlarged area corresponds to the first ~345 m of the studied sector. Red labels correspond to the approximate location of the photographs in Fig. 76. Cave survey by Marc Galy, Groupe Spéléologique des Pyrénées (GSPY 86).

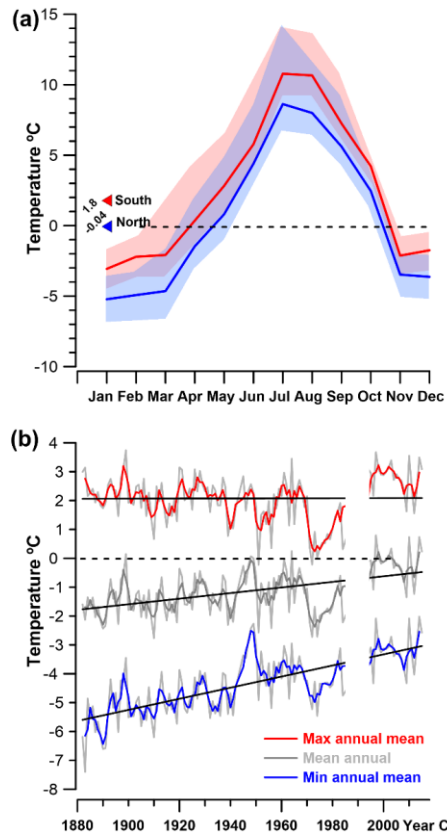


Figure 3. (a) Monthly temperature variation on the northern and southern side of the Monte Perdido massif. Red and blue triangles correspond to the 4-year means. The dashed black line indicates 0°C. Light red and blue shaded envelopes represent the maximum and minimum mean monthly temperatures, respectively. (b) Maximum, mean and minimum annual temperatures recorded at the Pic du Midi de Bigorre station since 1882. Black line indicates the general trend and dashed black line corresponds to 0°C.

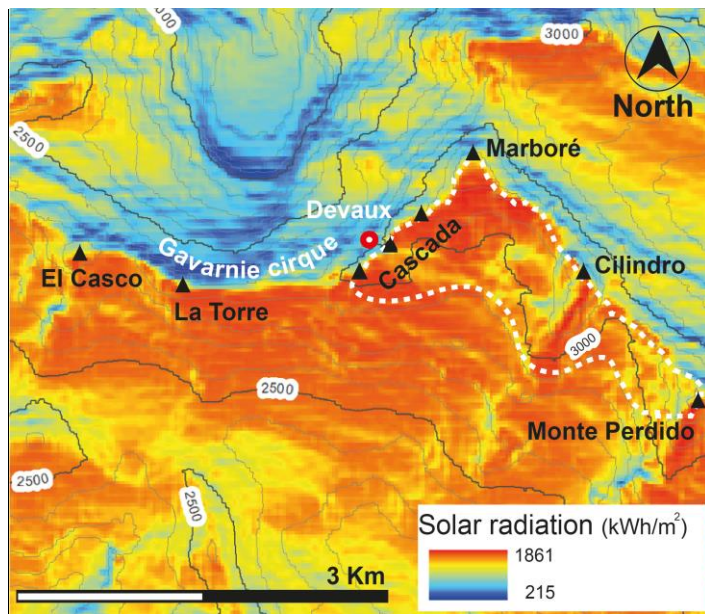


Figure 4. Solar radiation map of the study area. The solar radiation anomaly observed in the Gavarnie cirque is explained by its northerly orientation and the cirque morphology. Black triangles indicate the main peaks above 3000 m. The red-white circle marks Devaux cave, while the dashed white line delineates the approximate catchment.

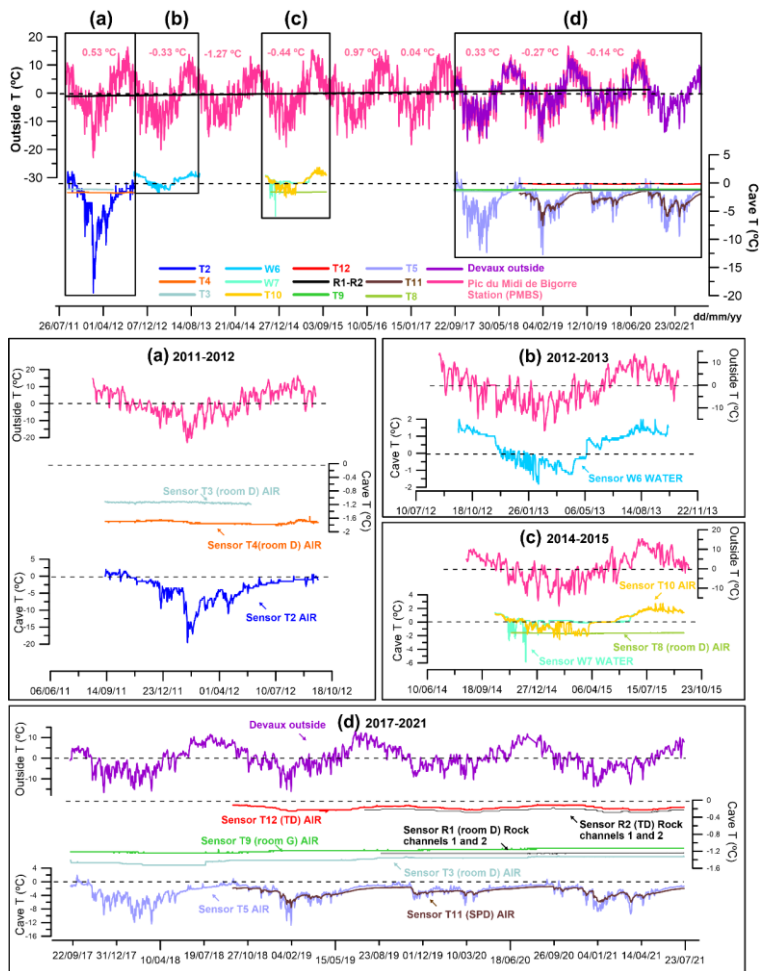


Figure 5. Mean daily air temperature variations at the Pic du Midi de Bigorre station (2860 m a.s.l., red), daily outside air temperature at Devaux cave (2836 m a.s.l., purple) and temperature variations in air, water and rock in the cave for the different time windows since 2011. Dark pink numbers are mean annual air temperatures (MAAT) at the Pic du Midi de Bigorre station (PMBS). Dashed lines indicate 0 °C. Black squares labelled a, b, c, and d correspond to the areas enlarged below. The black continuous line is the external temperature trend during the monitoring period.

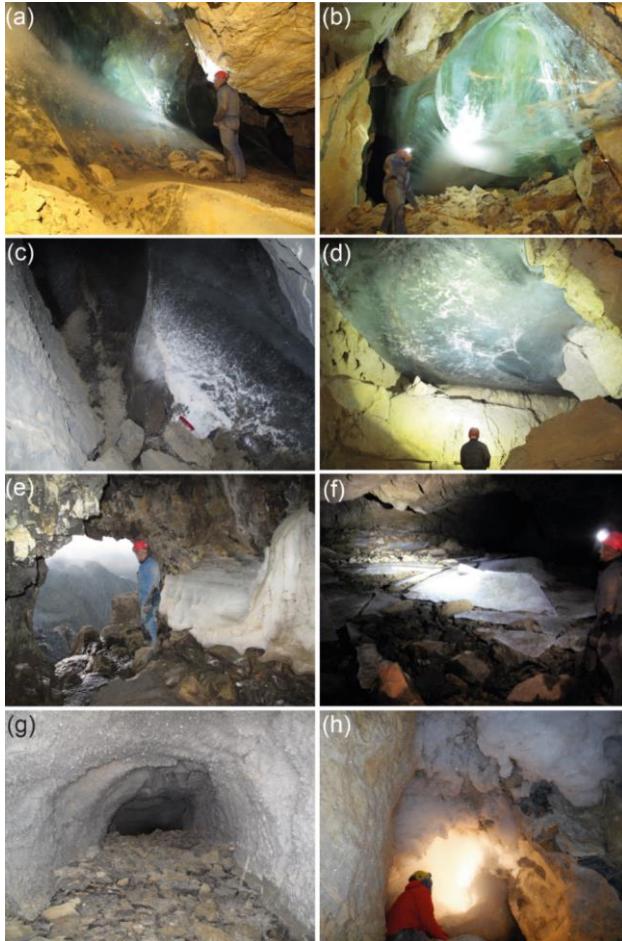


Figure 6. (a) Upper part of the ice body in room D. (b) Ice body hanging from the ceiling and the southwest wall in room G. White spots at near the bottom of the deposit correspond to the concentration of air inclusions as well as cryogenic carbonates and gypsum in the ice. (c) Small ice body in room SPD with CCC-CCG on and within the ice. Red knife (9 cm) for scale. (d) Ice body on the ceiling of room K (Terminus Devaux, TD). (e) Brulle spring and remains of a layered ice body (September 2018). (f) Broken ice sheets in the flooded area in room F (September 2018). (g) Millimetre to centimetre size perennial hoarfrost in a blind gallery below SPD room. (h) Seasonal hoarfrost aggregates (>30 cm long size) covering a cupola close to room J.

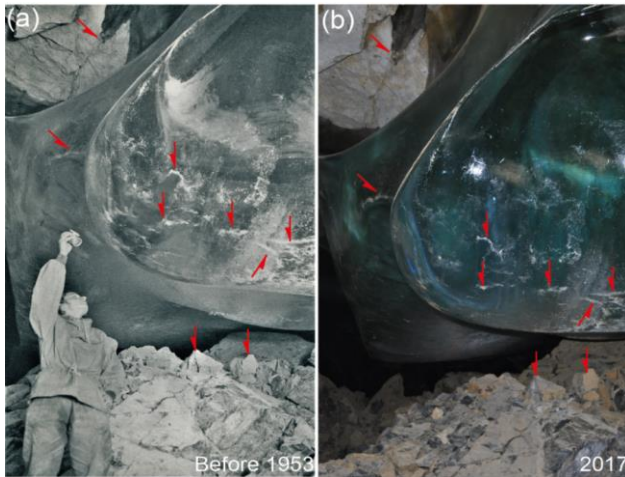


Figure 7. (a) Photo of the ice body located in room G [taken shortly](#) before 1953 ([Casteret, 1953](#)). (b) Photo taken in 2017. In both pictures, white patches on the ice surface correspond to small CCC accumulations released from the ice by sublimation. Red arrows indicate common features in both images.

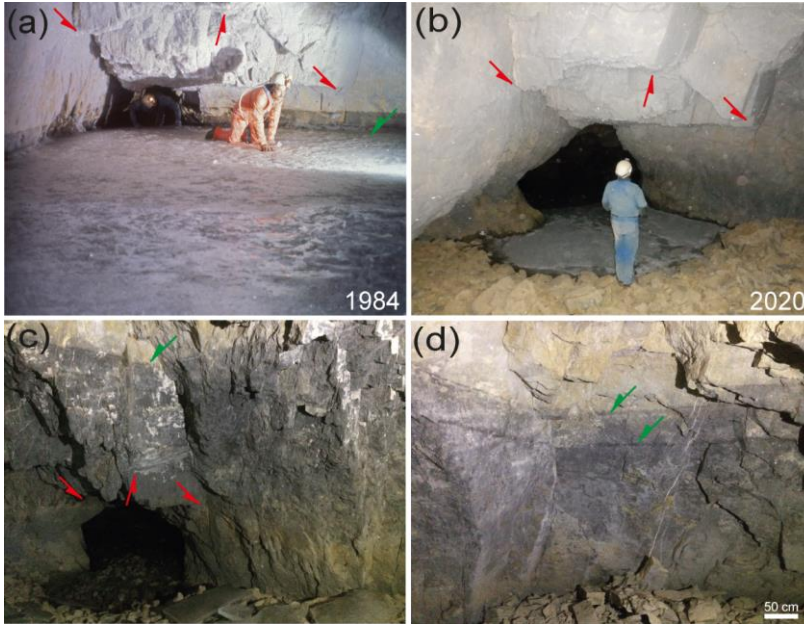


Figure 8. (a) Photo taken close to the river sector that connects the rooms F and E. The estimated ice level is 5 m higher than the Brulle spring. Photo by Jean Luc Bernardin (8th August 1984). (b) Similar area in 2020, and maximum extension of the seasonal lake ice formed during winter. (c) Higher ice mark level (c. +9.5 m with respect to the Brulle spring) and remnants of ice sheets from the frozen lake in 2018. (d) Two ice level marks (c. +9.2 m and +8.8 m with respect to the Brulle spring) located between the highest mark and the elevation of the ice in photo (a). In all images red arrows indicate the same rock edges, while green arrows show ice-level marks.

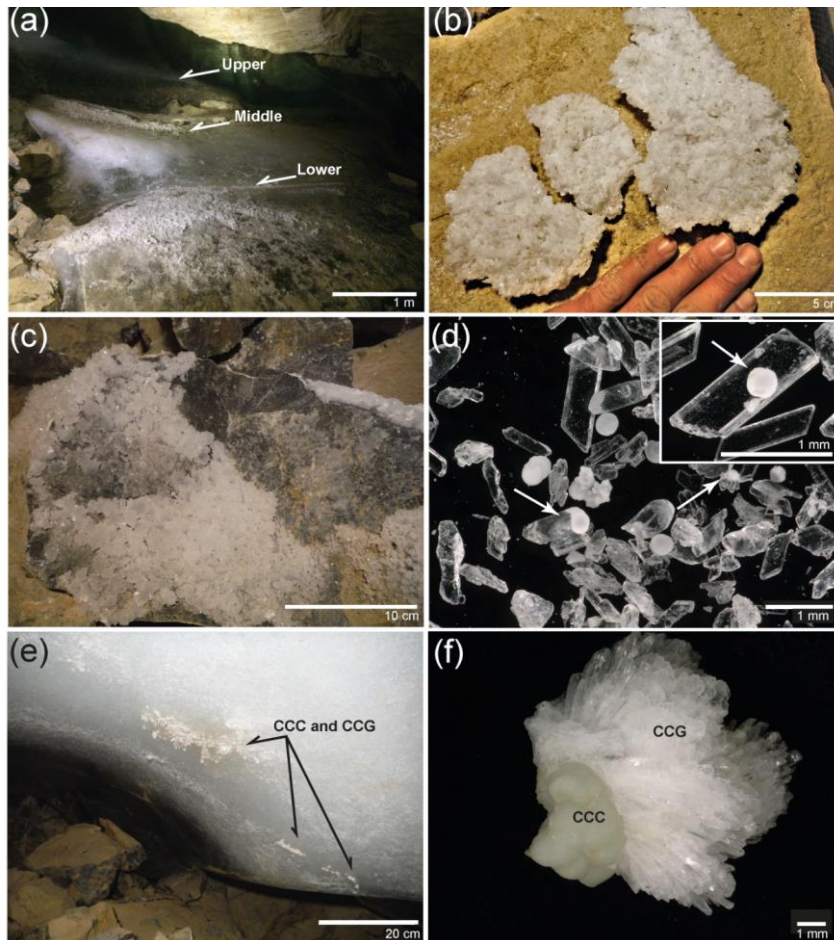


Figure 9. (a) Ice body in room G and three levels marked by cryogenic gypsum partially still in situ in the ice. The white area corresponds to milky ice with a high abundance of air inclusions. Gypsum crystals cover parts of the surface of the ice body due to ice retreat. (b) Large gypsum “raft” deposited on a block in room D. (c) Block in room D with gypsum overgrowths. (d) Microscopic image of euhedral CCG with ~~leaf~~ cores of CCC (white arrows), globular CCC, and ~~detail~~ [enlarged image](#) of euhedral gypsum crystal with a ~~core-nucleus~~ of globular CCC. (e) CCC and CCG entrapped within milky ice in room G. (f) Detail of a CCC sample from room G covered by CCG.

Date	Sample	Cations					Anions									
		Na ⁺	NH ₄ ⁺	K ⁺	Ca ²⁺	Mg ²⁺	F ⁻	Cl ⁻	NO ₂ ⁻	Br ⁻	NO ₃ ⁻	SO ₄ ²⁻	HCO ₃ ⁻	CO ₃ ²⁻	PO ₄ ³⁻	
15/09/2017	Devaux river 1	1.6	0.0	0.5	36.0	8.5	0.0	0.2	0.0	0.0	1.8	21.6	61.0	11.6	0.0	
	Devaux drip 1	0.9	0.1	0.5	50.5	18.2	0.1	0.5	0.0	0.0	6.8	67.4	95.2	0.0	0.0	
	Devaux drip 2	1.4	1.2	1.3	53.2	19.5	0.1	1.1	0.1	0.0	7.4	70.1	101.3	0.0	0.0	
22/07/2018	Devaux Ice 1 (room D)	2.3	0.0	0.3	24.8	2.7	0.1	1.3	0.0	0.0	0.7	19.0	23.9	1.0	0.0	
	Devaux Ice 2 (room D)	2.2	1.3	2.5	27.8	2.0	0.0	2.1	0.0	0.0	1.5	17.0	30.7	0.0	0.0	
	Devaux river 1	0.6	0.0	0.4	32.4	4.4	0.0	0.2	0.0	0.0	0.9	5.1	53.7	4.0	0.1	
22/09/2018	Devaux river 2	0.6	0.0	0.4	32.2	4.4	0.0	0.2	0.0	0.0	0.9	5.1	56.1	2.6	0.0	
	Devaux drip 1	1.4	0.0	3.2	61.0	20.8	0.2	2.2	0.0	0.0	14.1	76.0	84.2	5.6	0.0	
	Devaux drip 2	2.3	0.1	1.7	60.8	21.0	0.2	2.2	0.0	0.0	14.1	76.9	91.5	4.4	0.0	
28/07/2020	Devaux river 1*	1.3	0.0	0.4	40.5	7.9	0.0	0.3	0.0	0.0	2.0	17.0	65.9	0.0	0.0	
	Devaux drip 1*	1.6	0.0	1.2	70.6	27.2	0.2	1.1	0.0	0.0	19.8	116.5	90.3	0.0	0.0	
	Devaux ice (seasonal)*	0.4	0.0	0.5	28.2	1.1	0.1	0.5	0.0	0.0	0.5	2.8	36.6	0.0	0.0	
26/07/2021	Devaux river 1*	0.6	0.0	0.3	31.5	4.1	0.0	0.2	0.0	0.0	0.8	5.9	58.6	0.0	0.0	
	Devaux drip 1*	1.1	0.2	1.1	42.3	12.5	0.1	0.5	0.0	0.0	2.9	38.4	101.3	0.0	0.0	
	Devaux drip 2*	1.1	0.1	1.0	43.6	13.5	0.1	0.4	0.0	0.0	2.7	38.2	89.1	0.0	0.0	
13/08/2021	Devaux drip 3*	1.6	0.7	1.5	47.9	13.1	0.1	1.1	0.0	0.0	2.2	36.7	107.4	0.0	0.0	
	Devaux drip 1	2.9	0.0	1.1	83	35.9	0.3	5.9	0.6	0.1	40.2	269.3	104.9	0.0	0.0	
	Devaux drip 2	3.3	0.4	2.0	73.2	29.3	0.2	6.0	0.1	0.0	28.6	212	112.2	0.0	0.0	
26/07/2021	Devaux river 1	0.4	0.0	0.1	25.7	4.3	0.1	2.6	0.1	0.0	3.2	16.3	68.3	0.0	0.0	
	Devaux river 1	0.7	0.0	0.2	28.6	4.9	0.1	2.6	0.0	0.0	1.5	20.4	74.4	0.0	0.0	
	Devaux drip 1	7.5	2.2	5.1	49.5	15.2	0.2	10.3	0.3	0.0	6.9	77.3	130.5	0.0	0.0	
26/07/2021	Devaux drip 2	5.1	1.3	2.8	49.3	15.6	0.2	6.5	0.1	0.0	6.5	80.5	129.3	0.0	0.0	

Table 1. Chemical composition of water and ice samples from Devaux cave (in mg/l). * Samples where TDS (total dissolved solids) was calculated.

Location	Sample and description	$\delta^{34}\text{S}$ (‰) VCDT
Room D	Gypsum crystal (part of large raft)	-15.8
Room D	Gypsum crystal (part of large raft)	-15.5
Room D; lower gypsum level	Gypsum crystal (individual)	-15.6
Room D; middle gypsum level	Gypsum crystal (individual)	-15.0
Room D; middle gypsum level	Gypsum crystal (individual)	-15.6
Room D; upper gypsum level	Tiny gypsum crystals (aliquot)	-15.3
Room D	Gypsum crystal (individual)	-15.1
Room G	Gypsum crystal (individual)	-12.3
Room G	Gypsum overgrowth (individual)	-12.1
Room G	Gypsum overgrowth (individual)	-11.9
Room G	Gypsum overgrowth (individual)	-12.1
Room G	Gypsum overgrowth (individual)	-12.0
Limestone above cave	Pyrite crystal (individual)	-12.7
Entrance "Porche"	Drip water (1 liter)	-14.4
Bulle spring	River water 1 (1 liter)	-28.5
Bulle spring	River water 2 (1 liter)	-27.3

Table 2. Sulfur isotope values of gypsum, water and pyrite from Devaux.